

# The metallicities of luminous, massive field galaxies at intermediate redshifts.

M. Mouhcine<sup>1\*</sup>, S.P. Bamford<sup>2†</sup>, A. Aragón-Salamanca<sup>2</sup>, O. Nakamura<sup>2</sup>

<sup>1</sup>*Astrophysics Research Institute, Liverpool John Moores University, Twelve Quays House, Egerton Wharf, Birkenhead, CH41 1LD, UK.*

<sup>1</sup>*School of Physics and Astronomy, University of Nottingham, Nottingham, NG7 2RD, UK*

Accepted ?. Received ?; in original form ?

## ABSTRACT

We derive oxygen abundances for a sample of 40 luminous ( $M_B \lesssim -19$ ), star-forming, mostly disk, field galaxies with redshifts in the range  $0.2 \lesssim z \lesssim 0.8$ , with a median of  $\langle z \rangle = 0.45$ . Oxygen abundances, relative to hydrogen, of the interstellar emitting gas are estimated by means of the empirically calibrated strong emission line ratio technique. The derived  $12 + \log(\text{O}/\text{H})$  values range from 8.4 to 9.0, with a median of 8.7. Twenty of these galaxies have securely measured rotation velocities, in the range 50–244  $\text{kms}^{-1}$ .

The measured emission line equivalent widths and diagnostic ratios for the intermediate redshift galaxies cover similar ranges to those observed across a large sample of local galaxies. The estimated oxygen abundances for our luminous star-forming intermediate redshift galaxies cover the same range as their local counterparts. However, at a given galaxy luminosity, many of our galaxies have significantly lower oxygen abundances, i.e.,  $12 + \log(\text{O}/\text{H}) \sim 8.6$ , than local galaxies with similar luminosities. Interestingly, these luminous, massive, intermediate redshift, star-forming galaxies with low oxygen abundances exhibit physical conditions, i.e., emission line equivalent width and ionization state, very similar to those of local *faint* and metal-poor star-forming galaxies. The oxygen abundance of the interstellar gas does not seem to correlate with the maximum rotation velocity or the emission scale length of the parent galaxy. This suggests that there is a diversity in the intrinsic properties of the massive field galaxy population at intermediate redshifts.

The distribution of the colour excess, derived from the ratio of extinction-uncorrected  $\text{H}\beta$  and  $[\text{OII}]\lambda 3727$  star formation rate indicators, covers a similar range to that observed locally, but exhibits a lower mean than is observed for local optically-selected star-forming galaxies. Luminous field galaxies at intermediate redshifts show similar star formation rates to their local counterparts. However, metal-poor, massive, star-forming galaxies tend to be systematically less affected by internal reddening than metal-rich, massive galaxies, which cover similar range of colour excess to local metal-rich luminous galaxies. Finally, the correlation between oxygen abundance and colour excess for intermediate redshift galaxies is found to be similar to what is observed locally. This result indicates that the dust content of galaxies is more regulated by their chemical evolution rather than galaxy luminosity.

**Key words:** galaxies: evolution – galaxies: abundances – galaxies: fundamental parameters

## 1 INTRODUCTION

The chemical abundances of stars and interstellar gas within galaxies provide a fundamental tool for tracing the evolution of galactic chemical enrichment. Furthermore, the ratios of chemical element abundances help in constraining the star formation histories of galaxies. The determination of galactic

\* Isaac Roberts Fellow

† Current address: Institute of Cosmology and Gravitation, University of Portsmouth, Mercantile House, Hampshire Terrace, Portsmouth, PO1 2EG, UK.

chemical abundances at different cosmic epochs can thus assist in constraining the likely scenarios of galaxy evolution.

With the advent of 10-m class telescopes and their powerful optical and near-infrared spectrographs, it is now possible to probe the properties of the interstellar gas in intermediate ( $0 < z < 1$ ; Kobulnicky & Zaritsky 1999; Hammer et al. 2001; Lilly et al. 2003; Liang et al. 2004, Maier et al. 2004, Kobulnicky & Kewley 2004; Maier et al. 2005) and high-redshift ( $1.5 < z < 4$ ; Pettini et al. 1998, 2001; Kobulnicky & Koo 2000; Mehlert et al. 2002; Lemoine-Busserolle et al. 2003; Erb et al. 2003; Maier et al. 2006) galaxies. The classical nebular diagnostic techniques developed to study the properties of HII regions and emission line galaxies in the local universe are now used to study higher redshift galaxies (see Kobulnicky & Zaritsky 1999).

The correlation between galaxy metallicity and luminosity in the local universe is one of the most significant observational results in galaxy chemical evolution studies (e.g., Lequeux et al. 1979; Skillman et al. 1989; Zaritsky et al. 1994; Melbourne & Salzer 2002; Lamareille et al. 2004; Tremonti et al. 2004). Recent studies of galaxy evolution trace changes in scaling relations of galaxies as a function of cosmic epoch, such as the Tully–Fisher relation for disks (e.g., Simard & Pritchett 1998; Ziegler et al. 2002; Milvang-Jensen et al. 2003; Bamford et al. 2006; Nakamura et al. 2006) and the fundamental plane relation for spheroids (e.g., Im et al. 2002; van Dokkum & Ellis 2003). In this context, the evolution of the luminosity–metallicity relation of galaxies as a function of cosmic epochs can be used as a sensitive probe and consistency check of galaxy evolution.

The analysis of oxygen abundances of star-forming galaxies at intermediate redshifts seems to point toward the conclusion that the luminosity–metallicity relation evolves with redshift, with steeper slope at earlier cosmic time (Kobulnicky et al. 2003; Maier et al. 2004; Liang et al. 2004). Bright galaxies, with  $L \approx L_*$ , at intermediate redshift tend to have properties similar to bright galaxies in the local universe, and fall on the local luminosity–metallicity relation. However, faint galaxies seem to be systematically brighter for their metallicity in comparison to the local luminosity–metallicity relation. Lilly et al. (2003) found, however, that a significant fraction of a statistically complete sample of bright, i.e.,  $M_{B,AB} \leq -20$ , H $\beta$ -selected intermediate redshift galaxies appear to have low oxygen abundances, similar to what is seen in the local universe for galaxies with luminosities a factor of 10 or more lower. More recently, Maier et al. (2005) found that about one third of the Canada-France Redshift Survey galaxies they studied, with  $M_{B,AB} \leq -19.5$ , have significantly lower oxygen abundances than do local galaxies with similar luminosities.

Intermediate redshift galaxies with low oxygen abundances have bluer colours than higher metallicity ones. Lilly et al. (2003) argue that these galaxies are immature massive galaxies that will increase their oxygen abundances to the present epoch in a downsizing scenario – in which the manifestations of star-forming evolutionary activity appear in progressively more massive galaxies at earlier epochs – rather than dwarf galaxies with their luminosities boosted by ongoing star formation events. The appearance of a population of massive galaxies with low oxygen abundances at  $z \lesssim 1.0$  is consistent with a later stellar mass assembly for

a fraction of massive and intermediate-mass galaxies (Hammer et al. 2005).

The number of intermediate redshift galaxies with measured kinematics is relatively small. Bamford et al. (2005, 2006) and Nakamura et al. (2006) have extended the study of the kinematics of emission line galaxies at this redshift range by measuring the maximum rotation velocities for sizeable samples of luminous, i.e.,  $M_B \leq -19.5$ , cluster and field galaxies in the redshift range  $0.1 \lesssim z \lesssim 1.0$  (see the quoted papers for more details). In the present paper, we analyze the properties of the interstellar emitting gas of field galaxies in the Bamford et al. (2005, 2006) and Nakamura et al. (2006) samples. This will enable us to constrain the nature of the luminous galaxies with intermediate metallicities found at intermediate redshifts, and hence test the downsizing scenario for galaxy formation. The properties of cluster galaxies are analysed in another paper (Mouhcine et al. 2006).

The paper is organized as follows. In Section 2 we describe the sample selection and emission line measurements. Distributions of galaxy properties are presented and discussed in Section 3. In Section 4, we present the luminosity–metallicity relation, star formation rates, and interstellar extinction of our galaxy sample. The implications of our results are discussed in Section 5, and we summarize our conclusions in Section 6.

A concordance cosmological model with  $H_0 = 70 \text{ km s}^{-1}$ ,  $\Omega_\Lambda = 0.7$ ,  $\Omega_m = 0.3$  has been adopted throughout the paper.

## 2 OBSERVATIONS AND SAMPLE SELECTION

The target selection, photometry and spectroscopic data reduction have been described thoroughly elsewhere. Bamford et al. (2005) covers most of the VLT observations, Milvang-Jensen et al. (2003), Milvang-Jensen (2003) detail the VLT MS1054 data, and Nakamura et al. (2006) describes the Subaru observations. We therefore only briefly summarize this information here, before describing in more detail the equivalent width measurements utilized in this study.

The observed galaxies are located in nine fields, centred on galaxy clusters at redshifts in the range  $z = 0.20\text{--}0.83$ . Spectroscopy and imaging were obtained using FORS2<sup>1</sup> on the VLT (Seifert et al. 2000), and FOCAS<sup>2</sup> on the Subaru telescope (Kashikawa et al. 2002). The galaxies observed within each field were selected by assigning priorities based upon the likelihood of being able to measure a rotation curve. Higher priorities were assigned for each of the following: disky morphology, favourable inclination for rotation velocity measurement, known emission line spectrum, and available Hubble Space Telescope data. It is important to note that this priority ranking method preferentially selects bright, star-forming disc galaxies, and therefore we are not probing the average galaxy population. However, this sample is still useful in examining the evolution of the brightest star-forming disc galaxies (see Bamford et al. 2005).

The absolute rest-frame *B*-band magnitudes utilised in

<sup>1</sup> <http://www.eso.org/instruments/fors>

<sup>2</sup> <http://www.naoj.org/Observing/Instruments/FOCAS>

this study are derived from a collection of multi-band imaging. For each galaxy, the available observed apparent magnitudes were converted to apparent rest-frame  $B$ -band using colour- and  $k$ - corrections determined from the spectral energy distribution best-fitting the colour data. The bands available for each galaxy vary, and are listed in Table A1 of Bamford et al. (2005), along with the band upon which the rest-frame  $B$ -band magnitude is based. This is always the closest observed match to rest-frame  $B$  available. The magnitudes are corrected for Galactic extinction using the maps and conversions of Schlegel, Finkbeiner & Davis (1998), and for internal extinction (including face-on extinction of 0.27 mag), following the prescription of Tully & Fouque (1985). Note that variations in internal extinction levels, as investigated later in this paper, likely produce both random and systematic uncertainties of  $\sim 0.1$ – $0.2$  mag on this correction. However, these errors are comparable to those introduced through uncertainties in the inclination measurement, and in any case are generally smaller than the differences found below between our intermediate-redshift and local comparison samples. All magnitudes given in this paper are on the Vega zeropoint system. For further details see Bamford et al. (2005).

From the reduced two-dimensional spectra, individual sky- and continuum-subtracted emission line ‘postage stamps’ were extracted. In order to measure the rotation velocity ( $V_{\text{rot}}$ ) and emission scale lengths ( $r_{\text{d,spec}}$ ) each emission line was fitted independently using a program named ELFIT2PY, which is based on the algorithms of ELFIT2D by Simard & Pritchett (1998, 1999). In order to produce a single value of  $V_{\text{rot}}$  and  $r_{\text{d,spec}}$  for each galaxy the values for the individual lines are combined by a weighted mean. The final galaxy kinematic sample contains 145 galaxies, including both field and cluster galaxies.

In order to measure line equivalent widths and fluxes the two-dimensional spectra were averaged in the spatial direction to produce one-dimensional spectra. The spatial region used for each spectrum was determined by averaging the two-dimensional spectrum in the wavelength direction, fitting a symmetrical (Voigt) profile, and calculating the distance from the fit centre to where the profile falls to approximately 1% of its peak value. All lines were fit with a combination of Gaussians using the iterative AMOEBA minimization algorithm of the IRAF/STSDAS task NGAUSSFIT. Once the best-fitting parameters (i.e. continuum level, position, amplitude and full width at half maximum for a single line) are found, their uncertainties are estimated through a Monte-Carlo resampling technique. In this, twenty synthetic data realisations are created from the best-fitting function, with random noise added to each pixel corresponding to the provided error image. These synthetic spectra are then fit in the same manner as the true data, and the standard deviations of the resultant parameters are used to estimate the uncertainties on the best-fitting parameters for the true data.

Single Gaussian fits were attempted for all visible emission lines. Typically studies account for the effect of the underlying stellar Balmer lines in absorption by applying a correction to the rest-frame equivalent width of the  $H\beta$  emission line that is independent of the galaxy properties. Different correction values for  $H\beta$  stellar absorption have

been used in the literature, ranging from  $2\text{\AA}$  (e.g., Kobulnicky et al. 2003) to  $5\text{\AA}$  (e.g., Kennicutt 1992).

Balmer emission lines in the spectra of our galaxy sample have been corrected from the underlying stellar absorption by considering simultaneous fits of the emission and absorption lines. The two-component fits to the Balmer lines were found to be unreliable for a fraction of galaxy spectra, particularly for low  $S/N$  data. Figure 1 shows the difference in the emission line equivalent width measured from the two- and one-component fits ( $W_{\text{emi}}^{(2)}$  and  $W_{\text{emi}}^{(1)}$  respectively). This quantity is effectively the correction,  $\Delta W_{\text{emi}}^{+\text{abs}}(H\beta)$ , one would need to apply to the one-component fit emission line equivalent widths to obtain the true equivalent width in the absence of stellar absorption,

$$\Delta W_{\text{emi}}^{+\text{abs}}(H\beta) = W_{\text{emi}}^{(2)} - W_{\text{emi}}^{(1)}. \quad (1)$$

The one-component fits should underestimate the equivalent width in cases where Balmer line absorption is additionally present. The correction introduced by including this effect, namely through a two-component fit, typically amounts to  $\sim 2\text{\AA}$ . It can be seen that there is a ridge around  $\Delta W_{\text{emi}}^{+\text{abs}}(H\beta)$  at high  $S/N$ , and very large scatter at low  $S/N$ . However, highly deviant points continue to be present upto fairly high  $S/N$ . Virtually all of these outlying points are due to a failure of the two-component fit. The nature of the two-component fit makes it prone to fitting noise features either side of the emission line using a very deep absorption line, and hence requiring an overly large emission component to still fit the central emission line. However, when attempting to fit noise features the best-fitting parameters naturally have high uncertainties. In order to identify unreliable two-component fits we estimate the additional error introduced into the equivalent width measurement by the inclusion of the absorption component as

$$\sigma_{W,\text{emi}}^{+\text{abs}} = \sqrt{\sigma_{W,\text{emi}}^{(2)2} - \sigma_{W,\text{emi}}^{(1)2}}. \quad (2)$$

A plot of  $\Delta W_{\text{emi}}^{+\text{abs}}(H\beta)$  versus  $\sigma_{W,\text{emi}}^{+\text{abs}}$  does a considerably better job of separating points with reasonable  $\Delta W_{\text{emi}}^{+\text{abs}}(H\beta)$  values from those with unrealistically high  $\Delta W_{\text{emi}}^{+\text{abs}}(H\beta)$ , as can be seen in Figure 2.

From examining Figure 2, it is clear that points with  $\sigma_{\text{EW,emi}}^{+\text{abs}} < 1.0\text{\AA}$  nearly all lie around the value of  $\sim 2\text{\AA}$ . For  $\sigma_{\text{EW,emi}}^{+\text{abs}}$  above this value there is a striking increase in both the scatter, and the number of unrealistically discrepant points. Note that  $\sigma_{\text{EW,emi}}^{+\text{abs}} < 1.0\text{\AA}$  corresponds to where the uncertainty contributed by the inclusion of an absorption component in the fit is less than half the expected size of the correction. That is, at  $\sigma_{\text{EW,emi}}^{+\text{abs}} > 1.0\text{\AA}$  we would expect  $> 10\%$  of points to lie further from the true value of the correction than the size of the correction itself, simply due to the measurement uncertainty. It therefore seems reasonable to only consider two-component fits for which  $\sigma_{\text{EW,emi}}^{+\text{abs}} < 1.0\text{\AA}$ . In addition, a cut on  $\Delta W_{\text{emi}}^{+\text{abs}}(H\beta)$  is also useful in order to discard clearly discrepant points with  $\Delta W_{\text{emi}}^{+\text{abs}}(H\beta) > 5\text{\AA}$ . These cuts are indicated in Figure 2.

The mean of  $\Delta W_{\text{emi}}^{+\text{abs}}(H\beta)$  for spectra with both reliable two- and one-component fits to  $H\beta$  is  $1.9\text{\AA}$ , with scatter  $0.9\text{\AA}$ . Accounting for measurement uncertainties leaves an intrinsic scatter about the mean of  $\sim 0.6\text{\AA}$ . For galaxies with reliable two-component Balmer fits we use the emis-

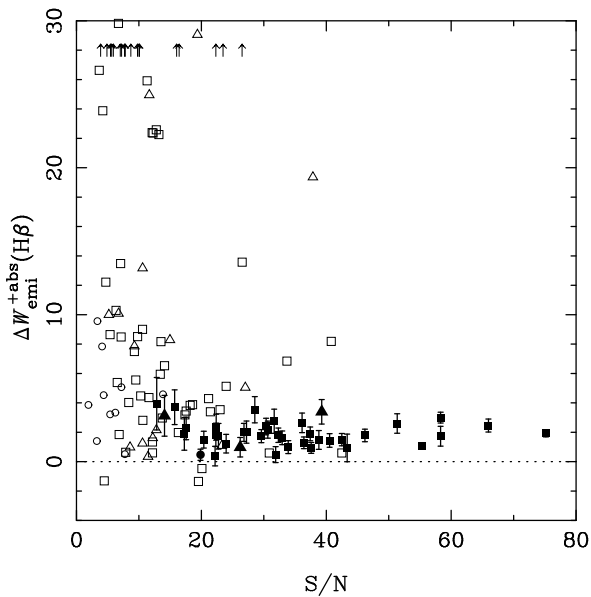


**Figure 1.** The  $H\beta$  absorption correction,  $\Delta W_{\text{emi}}^{+\text{abs}}(H\beta)$ , determined from the difference between the emission line equivalent width measurements of two-component and one-component fits, plotted versus the signal-to-noise in the adjacent continuum,  $S/N$ . The filled points are those which have robust two-component fits, as judged by the cuts described in the text and indicated in Figure 2. Error bars are omitted from the open points for clarity.

sion equivalent width determined from this fit. For all other galaxies we use the result of the one-component fit, and apply a uniform correction for the effect of stellar absorption. For this correction we adopt the mean of that determined for the two-component fits,  $\langle \Delta W_{\text{emi}}^{+\text{abs}}(H\beta) \rangle = 1.9\text{\AA}$ , and include an additional uncertainty of  $0.6\text{\AA}$  in quadrature.

Our entire sample of field galaxies with identifiable emission lines contains 212 galaxies, and spans a redshift range of 0.04 to 1.22 with a median of 0.36. We searched within this spectroscopic sample for galaxies with emission lines suitable for chemical analysis. Only galaxies for which it was possible to measure  $[\text{OII}]\lambda 3727$ ,  $H\beta$ , and  $[\text{OIII}]\lambda 5007$  emission lines were retained, i.e., the lines needed to determine the ionizing source and to measure the oxygen abundance. After applying these selection criteria the sample size drops to 60. For reliable oxygen abundance determinations, only galaxies for which  $H\beta$  emission line is well detected are retained. This was judged by requiring the  $S/N$ , estimated from the median pixel value in regions  $29\text{--}58\text{\AA}$  away from the line on both sides, divided by the median value of the error image in the same region, to be larger than 8. An additional 16 objects were excluded from the sample due to the weak detection of  $H\beta$ . Of the the original data set with 212 objects, the final sample contains 44 emission line galaxies. Twenty-one of the sample galaxies have securely measured rotation velocities.<sup>3</sup>

<sup>3</sup> These numbers reduce to 40 and 20 respectively once four galaxies are rejected due to difficulties in measuring their metallicities; see section 4.1.

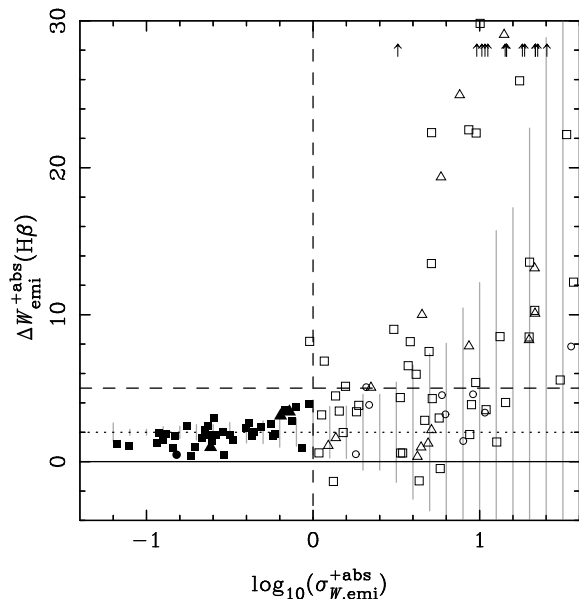


**Figure 2.** The  $H\beta$  absorption correction,  $\Delta W_{\text{emi}}^{+\text{abs}}(H\beta)$ , determined from the difference between the emission line equivalent width measurements of two-component and one-component fits, plotted versus an estimate the additional error introduced into the EW measurement by the inclusion of the absorption component,  $\sigma_{\text{EW,emi}}^{+\text{abs}}$ . Measurements from the 2002 VLT data are plotted with squares, the 2001 VLT data are plotted with circles, and Subaru data are plotted using triangles. Dashed lines show the cuts adopted in selecting the reliable sample of two-component fits. Those points which pass these cuts are filled, while those rejected are open. The mean  $\Delta W_{\text{emi}}^{+\text{abs}}(H\beta)$  of the reliable points, used to correct the one-component  $H\beta$  fits for the effects of stellar absorption, is indicated by the dotted line. The gray vertical lines indicate the average error on the data points, in bins of 0.1 dex in  $\sigma_{\text{EW,emi}}^{+\text{abs}}$ .

### 3 SPECTRAL ANALYSIS

#### 3.1 Contamination from active galactic nuclei

Nonthermal sources, such as active galactic nuclei (AGN), often produce emission-line spectra that superficially resemble those of star-forming regions. AGN must be identified as such because blindly applying emission-line metallicity diagnostics calibrated from HII region photoionization models will produce erroneous metallicities.

Traditionally, AGN can be distinguished from star-forming galaxies using the classical diagnostic ratios of two pairs of relatively strong emission lines, i.e.,  $[\text{OIII}]\lambda 5007/H\beta$  vs.  $[\text{NII}]\lambda 6584/H\alpha$ , and/or  $[\text{OIII}]\lambda 5007/H\beta$  vs.  $[\text{SII}]\lambda 6717, \lambda 6731/H\alpha$  diagrams (Baldwin et al. 1981, Veilleux & Osterbrock 1987). Some of these emission lines are usually not available for galaxies at  $z \gtrsim 0.3$ . To solve this Rola et al. (1997) have investigated the location of starbursts and AGNs in diagnostic diagrams involving *blue* emission lines only, i.e.  $[\text{OII}]\lambda 3727$ ,  $H\beta$ , and  $[\text{OIII}]\lambda 4959$  (see also Dessauges-Zavadsky et al. 2000). More recently, Lamareille et al. (2004) have used a large sample of emission line galaxies drawn from the Two Degree Field Galaxy Redshift Survey to investigate the separation between starbursts and AGNs using equivalent width ratios of blue emission line ratios as diagnostics for the ionizing source.

None of the observed spectra contain all the required emission lines to determine the ionizing source using the classical techniques. Thus, we use the equivalent width ratios of  $[\text{OIII}]\lambda 4959, \lambda 5007/\text{H}\beta$  and  $[\text{OII}]\lambda 3727/\text{H}\beta$  as parametrized by Lamareille et al. (2004) to check for the presence of AGNs in our sample. Fig. 3 shows the distribution of the sample of intermediate redshift field galaxies in this diagnostic diagram. The solid curve shows the demarcation line, separating starburst galaxies from AGN, of Lamareille et al. (2004). All the objects in our sample fall within the zone where starburst galaxies are located, indicating that in all of them the source ionizing the interstellar gas is an episode of star formation. Table 1 lists the coordinates of the final sample of field galaxies.

### 3.2 Basic sample properties

Table 2 lists the redshifts, absolute B-band magnitudes,  $[\text{OII}]\lambda 3727, \text{H}\beta$ , and  $[\text{OIII}]\lambda 5007$  emission line equivalent widths, maximum rotation velocities, and emission scale length for the objects in our final sample.

The dashed line in Fig. 3 shows the theoretical sequence of McCall, Rybski, & Shields (1985) for line ratios of HII galaxies as a function of metallicity, which nicely fits measurements of local HII galaxies. The track is interpreted as a metallicity-excitation sequence; along the track the metallicity is high at the lower left, i.e., for low excitation systems, and low at the upper right, i.e., for high excitation systems (McCall et al. 1985). Intermediate redshift emission-line galaxies define a continuous sequence, strikingly consistent with that defined by local HII galaxies. Our sample contains objects with a wide variety of excitation levels, extending from those observed for local luminous galaxies to levels observed for faint and metal-poor dwarf galaxies at the present epoch. This might suggest that our sample of intermediate redshift, luminous, star-forming field galaxies contains both low-metallicity and metal-rich systems.

The upper panels of Fig. 4 show the distribution of redshift, B-band absolute magnitude, rotation velocity, and emission scale length for the final sample of intermediate redshift star-forming galaxies. The dashed histograms show the distribution of redshift and B-band absolute magnitude for galaxies with measured rotation velocities. Our sample of star-forming galaxies at intermediate redshifts is dominated by bright ( $M_B \lesssim -19$ ), massive ( $V_{\text{rot}} \gtrsim 80 \text{ km s}^{-1}$ ), and large disk galaxies ( $r_{\text{d,spec}} \gtrsim 2 \text{ kpc}$ ). The lower panels of Fig. 4 show the Tully–Fisher relation and the galaxy magnitude–size relation for our sample (see Bamford et al. 2005, 2006 and Nakamura et al. 2006 for more details). The redshift versus galaxy luminosity relation displays a correlation, i.e., only high luminosity galaxies are observed at higher redshift, while low-luminosity galaxies are detected mostly at low redshifts. Our galaxy sample is therefore biased toward brighter galaxies at the highest end of the redshift distribution. This is a type of selection bias expected for flux-limited spectroscopic surveys. The bottom right panel of Fig. 4 shows the relationship between the rest-frame equivalent widths of  $[\text{OII}]\lambda 3727$  and  $\text{H}\beta$  emission lines for our sample of intermediate redshift star-forming galaxies, shown as filled circles, and a comparative local sample of star-forming galaxies, shown as open circles (see Section 3.3 for more details). This figure shows that the overall distribu-

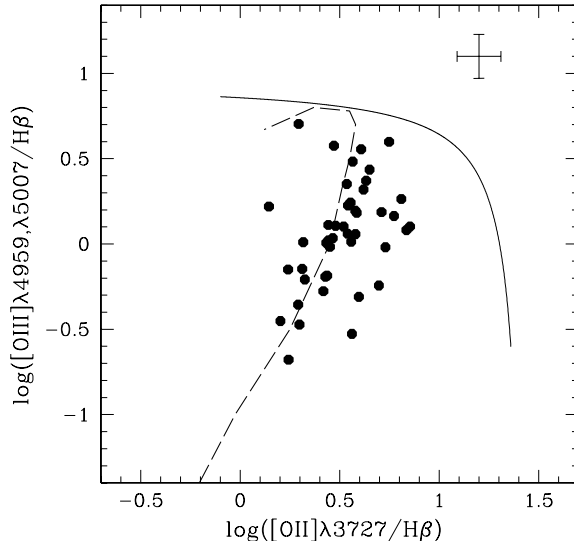


**Figure 3.** Diagnostic diagram for our sample of intermediate redshift emission line galaxies. The solid line shows the proposed separation between starburst galaxies and AGNs by Lamareille et al. (2004). The dashed line indicates the theoretical sequence of McCall et al. (1985), which fits the local HII regions with metallicity increasing from right to left.

tion of  $[\text{OII}]\lambda 3727$  rest-frame equivalent width for massive and luminous star-forming galaxies at intermediate redshifts is similar to the distribution for local star-forming galaxies.

### 3.3 Diagnostic diagrams

Different emission line ratios are sensitive to the metallicity and the level of ionization of the emitting gas, and may be used to probe the physical conditions of interstellar star-forming gas.

As a local galaxy sample to compare the properties of intermediate redshift galaxies with, and thus to investigate variation in the properties of star-forming galaxies between  $z \sim 0.5-1.0$  and the present epoch, we use the sample of Jansen et al. (2000), who observed the Nearby Field Galaxy Sample (NFGS) of about 200 galaxies. The galaxy sample was selected from the first CfA redshift catalog (Huchra et al. 1983) to approximate the local galaxy luminosity function. The NFGS sample includes galaxies of all morphological types and spans 8 mag in luminosity and a broad range of environments. The spectra of NFGS sample galaxies are integrated over a significant fraction of the galaxies, and are thus similar to the unresolved spectra of the intermediate redshift galaxies in our sample. Following Jansen et al. (2000), an additional correction for stellar absorption of  $1.5 \text{ \AA}$  ( $1 \text{ \AA}$ ) has been applied to the NFGS  $\text{H}\alpha$  ( $\text{H}\beta$ ) equivalent widths.

We use the classical diagnostic ratios of two pairs of relatively strong emission lines (Baldwin et al. 1981; Veilleux & Osterbrock 1987) to distinguish between galaxies dominated by emission from star-forming regions and galaxies dominated by emission from non-thermal ionizing sources. We classify galaxies according to their position in

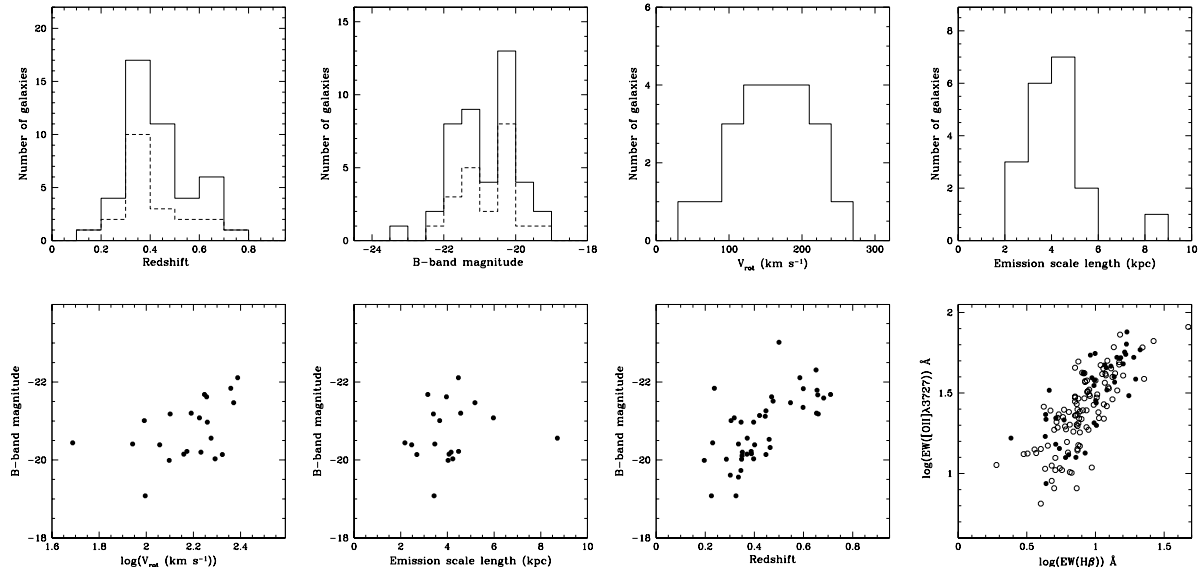


**Figure 4.** Upper panels: distribution of redshift, B-band absolute magnitude, rotation velocity, and emission length scale for our final sample of star-forming galaxies. Dashed histograms show the distribution of galaxies with measured maximum rotation velocity. Bottom panels: plots of maximum rotation velocity, emission scale length, and redshift versus B-band magnitude. The right panel shows the correlation between the rest frame equivalent widths of [OII] $\lambda$ 3727 and H $\beta$  emission lines for our intermediate redshift galaxy sample, shown as filled circles, and a local comparative sample from Jansen et al (2000); see text for more details.

[OIII] $\lambda$ 5007/H $\beta$  vs. [NII] $\lambda$ 6584/H $\alpha$  and [OIII] $\lambda$ 5007/H $\beta$  vs. [SII] $\lambda$ 6717,  $\lambda$ 6731/H $\alpha$  diagrams. The demarcation between star-forming galaxies and AGNs in both diagrams was taken from Kewley et al. (2001). We used the conservative requirement that a galaxy must be classified as a star-forming galaxy in both diagnostic diagrams in order to be retained in the local comparison sample of star-forming galaxies.

The colour excess from obscuration by dust for NFGS sample galaxies was estimated from the observed ratio of H $\alpha$  and H $\beta$  line fluxes. We adopt the Milky Way interstellar extinction law of Cardelli, Clayton, & Mathis (1989), with  $R_V = 3.1$ . We assume an intrinsic ratio Balmer decrement of 2.85, corresponding to the case B recombination with a temperature of  $T = 10^4$ K and a density of  $n_e \sim 10^2 - 10^4 \text{ cm}^{-2}$  (Osterbrock 1989). The published extinction laws are similar in the optical, making the determination of the colour excess independent of the exact choice of the extinction law.

The left panel of Fig. 5 shows the relationship between galaxy absolute B-band magnitude and [OII] $\lambda$ 3727 rest-frame emission line equivalent width. Galaxies in our sample are shown as filled circles, and the local star-forming galaxies in the NFGS sample are shown as open circles. The NFGS galaxies in this figure shows the well-established correlation between galaxy luminosity and emission line equivalent width, i.e., the bright end of the galaxy luminosity function at the present epoch is dominated by galaxies with low emission line equivalent width (e.g., Salzer et al. 1989; Kong et al. 2002; Jansen et al. 2000). Intermediate redshift star-forming galaxies in our sample cover a similar range of [OII] $\lambda$ 3727 rest-frame emission line equivalent width to that observed locally, but over a much narrower luminosity range, i.e.,  $\sim 2$  mag in comparison to the  $\sim 7$  mag covered by the NFGS sample. Strikingly, a fraction of massive and luminous field galaxies at intermediate redshifts show large

equivalent widths that are seen locally only for faint, i.e.,  $M_B \gtrsim -18$ , (and metal-poor) galaxies (see also Lilly et al. 2003).

Locally, faint and metal-poor galaxies that show large emission line equivalent widths tend to be highly ionized, while bright and metal-rich galaxies are characterized by low-ionization parameters (e.g., McCall et al. 1985; Stasińska 1990; Mouhcine et al. 2005). The right panel of Fig. 5 shows the relationship between [OII] $\lambda$ 3727 emission line rest-frame equivalent width and the diagnostic ratio [OIII] $\lambda$ 4959,  $\lambda$ 5007/[OII] $\lambda$ 3727. The line ratio [OIII] $\lambda$ 4959,  $\lambda$ 5007/[OII] $\lambda$ 3727 is a function of both ionization parameter and metallicity (Kewley & Dopita 2002).

The [OIII] $\lambda$ 4959,  $\lambda$ 5007/[OII] $\lambda$ 3727 ratio has been estimated using emission line equivalent widths. Kobulnicky & Phillips (2003) have shown that estimates of this ratio using equivalent widths give results similar to using emission line fluxes.

To illustrate the effect of galaxy luminosity (and hence metallicity for local galaxies, through their well established metallicity-luminosity relation) on the diagnostic ratio [OIII] $\lambda$ 4959,  $\lambda$ 5007/[OII] $\lambda$ 3727, we split the local sample of star-forming galaxies into faint ( $M_B > -19.5$ ) and bright ( $M_B \leq -19.5$ ), samples. The right panel of Fig. 5 shows that local star-forming galaxies are distributed along a well-defined sequence, interpreted as a metallicity-excitation sequence, with metallicity decreasing as the excitation parameter increases (e.g., Stasińska 1990). Intermediate redshift galaxies in our sample cover a similar range of [OIII] $\lambda$ 4959,  $\lambda$ 5007/[OII] $\lambda$ 3727 diagnostic ratio as is observed for local star-forming galaxies. In addition, star-forming galaxies in our sample are distributed similarly to local star-forming galaxies in the [OII] $\lambda$ 3727 rest-frame equivalent width vs. the diagnostic ratio

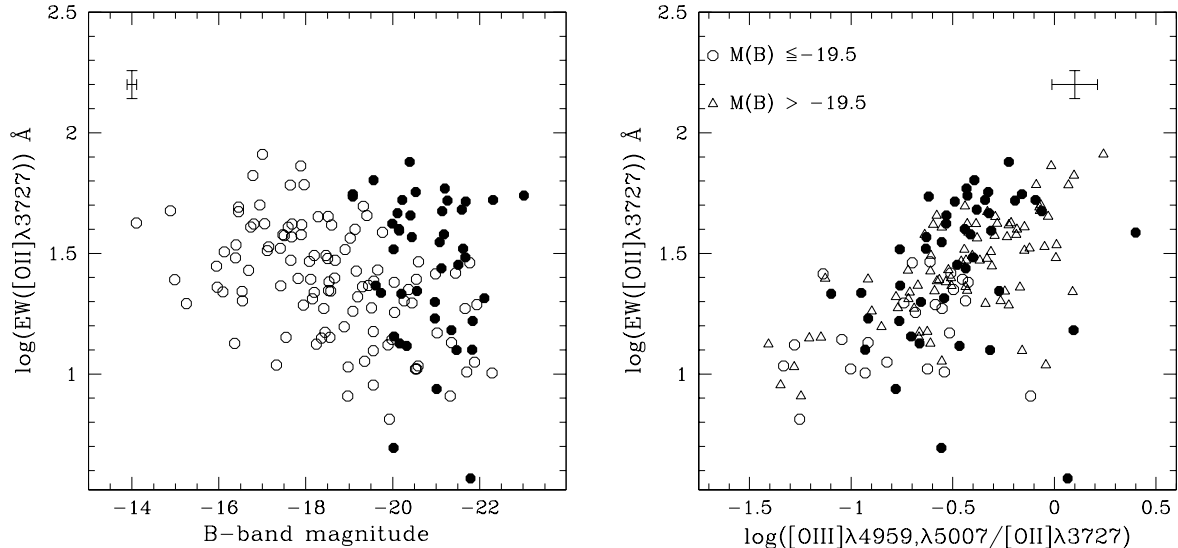


**Figure 5.** *Left:* The relationship between rest-frame  $[\text{OII}]\lambda 3727$  emission line equivalent width and B-band absolute magnitude for the sample of intermediate redshift star-forming galaxies (filled circles), and the NFGS sample of local star-forming galaxies (open circles). The figure shows clearly that a fraction of intermediate redshift galaxies show large  $[\text{OII}]\lambda 3727$  equivalent widths, observed only for faint galaxies at the present epoch. *Right:* The relationship between rest-frame  $[\text{OII}]\lambda 3727$  emission line equivalent width as a function of the excitation-sensitive diagnostic ratio  $[\text{OIII}]\lambda 4959, \lambda 5007 / [\text{OII}]\lambda 3727$ . Field star-forming galaxies at intermediate redshifts are shown as filled circles, open triangles show faint, i.e.,  $M_B > -19.5$ , NFGS galaxies, and open circles show bright, i.e.,  $M_B < -19.5$ , NFGS galaxies. The figure shows that a fraction of galaxies in our sample occupy the same region as local faint, metal-poor, star-forming galaxies.

$[\text{OIII}]\lambda 4959, \lambda 5007 / [\text{OII}]\lambda 3727$  diagram. Interestingly, however, a sub-sample of luminous star-forming galaxies at intermediate redshifts exhibit  $[\text{OIII}]\lambda 4959, \lambda 5007 / [\text{OII}]\lambda 3727$  ratios that are seen for much fainter local galaxies. This suggests that the physical parameters of the interstellar star-forming gas within luminous intermediate redshift, star-forming galaxies, i.e., their metallicity and ionization conditions, might be similar to those observed for fainter galaxies that are actively forming stars at the present epoch. This behaviour seems to extend to higher redshifts. Indeed, Maier et al. (2006) have shown that  $z \sim 1.4$  luminous star-forming galaxies exhibit much higher  $[\text{OIII}]\lambda 4959, \lambda 5007 / [\text{OII}]\lambda 3727$  ratios than galaxies with similar luminosities at  $0.4 \lesssim z \lesssim 0.9$ . Comparable  $[\text{OIII}]\lambda 4959, \lambda 5007 / [\text{OII}]\lambda 3727$  ratios are found only for much fainter star-forming galaxies at this lower redshift range. These constraints on the redshift evolution of ionization conditions of the interstellar star-forming gas, i.e., galaxies with a given  $[\text{OIII}]\lambda 4959, \lambda 5007 / [\text{OII}]\lambda 3727$  ratio are found to be brighter at earlier times, support the downsizing scenario for galaxy formation (see also Maier et al. 2006; see Sect. 5 for more details).

The ratio of hydrogen recombination lines to collisionally excited lines observed in one or more ionization states of oxygen is used as an abundance-sensitive ratio (e.g., Pagel et al. 1979). Fig. 6 shows the relationship between the most commonly used abundance-sensitive ratio  $([\text{OIII}]\lambda 4959, \lambda 5007 + [\text{OII}]\lambda 3727) / \text{H}\beta$ , the so-called  $R_{23}$  parameter (see Section 4.1 for more details) and B-band absolute magnitude for both local star-forming galaxies from the NFGS sample and our sample of intermediate redshift field galaxies. The solid line is the linear fit to the NFGS galaxy

sample (Jansen et al. 2001). Again, the measured  $R_{23}$  parameter for intermediate redshift star-forming galaxies cover a similar range to that observed for local star-forming galaxies.

Locally, the abundance-sensitive  $R_{23}$  parameter is correlated with metallicity, i.e., bright galaxies tend to have on average lower  $R_{23}$  parameters than faint galaxies. However, galaxies in our sample show a large scatter of  $R_{23}$  parameter at a given galaxy luminosity. Thus, unlike the local sample of star-forming galaxies, the sample of star-forming field galaxies at intermediate redshift contains luminous and massive objects with large  $R_{23}$  parameters, which are found locally only at lower luminosities, and are indicative of low oxygen abundances.

The observed excitation- and abundance-sensitive diagnostic ratios for star-forming galaxies in our sample are similar to what is exhibited by local galaxies over much larger luminosity and abundance ranges, i.e., from faint/metal-poor to luminous/metal-rich star-forming galaxies. The observed large variation of the interstellar ionized gas properties within luminous field galaxies at intermediate redshift suggests that these galaxies do not represent a homogeneous population of galaxies in terms of the physical properties that shape emission-line galaxy spectra, e.g., the ionizing stellar populations and the metal content. This indicates a sizeable evolutionary change of the properties of massive galaxies between  $z \sim 0.5$  and the present epoch.

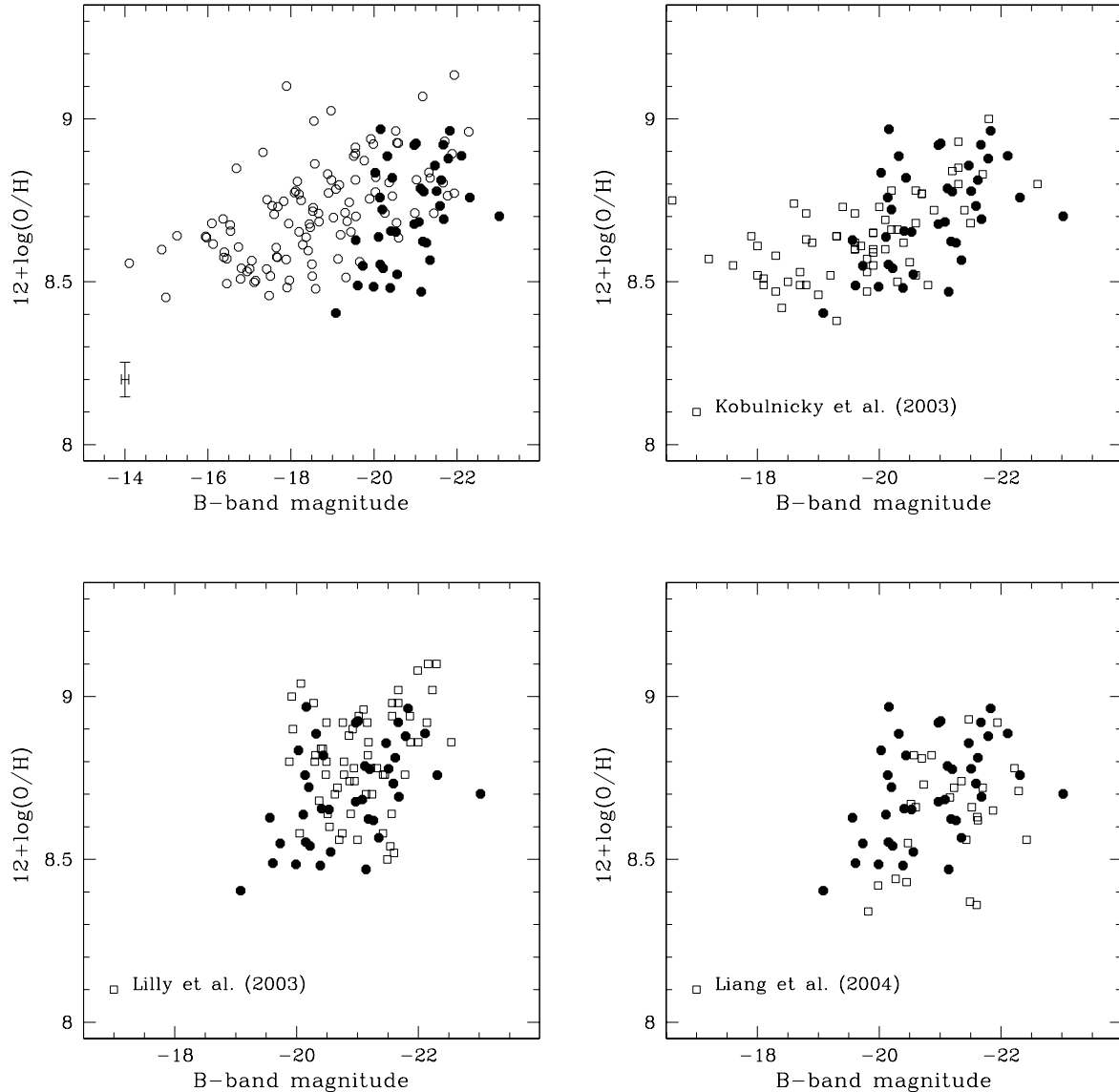


**Figure 8.** Luminosity–metallicity relation for our sample of intermediate redshift star-forming galaxies (filled circles), compared with several other samples, shown as open symbols. The comparison samples are: (upper-left) local star-forming galaxies from the NFGS sample; (upper-right) intermediate redshift galaxies,  $0.4 < z < 0.82$ , from Kobulnicky et al. (2003); (lower-left) the galaxy sample of Lilly et al. (2003), with  $0.47 < z < 0.92$ ; and (lower-right) luminous infrared galaxies with  $0.4 < z < 1.16$  from Liang et al. (2004). Oxygen abundances have been estimated assuming that all star-forming galaxies are on the upper-branch of the relationship between  $R_{23}$  parameter and  $12 + \log(\text{O}/\text{H})$  (see text for more details).

## 4 PROPERTIES OF LUMINOUS, MASSIVE INTERMEDIATE REDSHIFT GALAXIES

### 4.1 Gas phase oxygen abundances

The most reliable method of deriving the gas-phase oxygen abundance employs an estimate of the electronic temperature and density of the ionized gas (Osterbrock 1989). An accurate determination of these parameters requires reliable measurements of temperature-sensitive auroral lines, usually the  $[\text{OIII}]\lambda 4363$  emission line. Unfortunately, the observed spectra do not have the required signal-to-noise to correctly measure this line.

The absence of directly detected auroral lines, particularly in the case of metal-rich galaxies where these lines are too weak to be observed, requires the development of alternative methods based on strong emission lines. The most widely used method is based on measurements of  $[\text{OII}]\lambda 3727$ ,  $[\text{OIII}]\lambda 4959$ ,  $\lambda 5007$ , and  $\text{H}\beta$ . These lines contain enough information to get an accurate estimate of the oxygen abundance (McGaugh 1991). This is done through the parameter  $R_{23}$  introduced initially by Pagel et al. (1979), and defined as follows:

$$R_{23} = \frac{[\text{OIII}]\lambda 4959, \lambda 5007 + [\text{OII}]\lambda 3727}{\text{H}\beta} \quad (3)$$



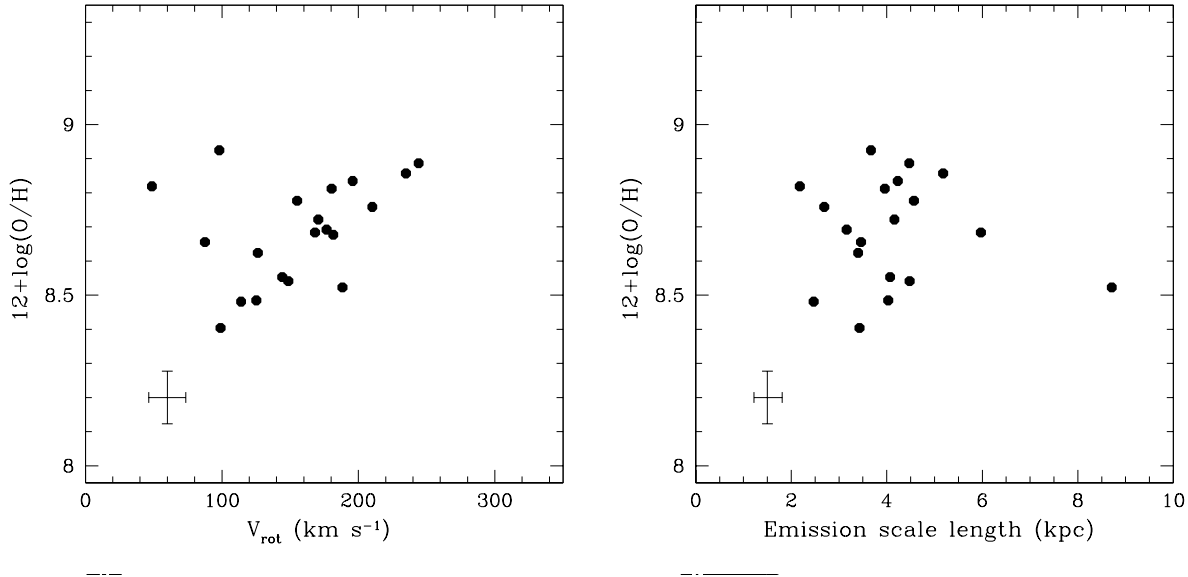


**Figure 9.** Relationship between oxygen abundance in terms of  $12 + \log(\text{O}/\text{H})$ , estimated using  $R_{23}$  parameter and assuming that all star-forming galaxies lie on the upper branch of  $R_{23}$  vs.  $12 + \log(\text{O}/\text{H})$  calibration, and maximum rotation velocity (left panel), and galaxy size (right panel). No convincing correlations are seen.

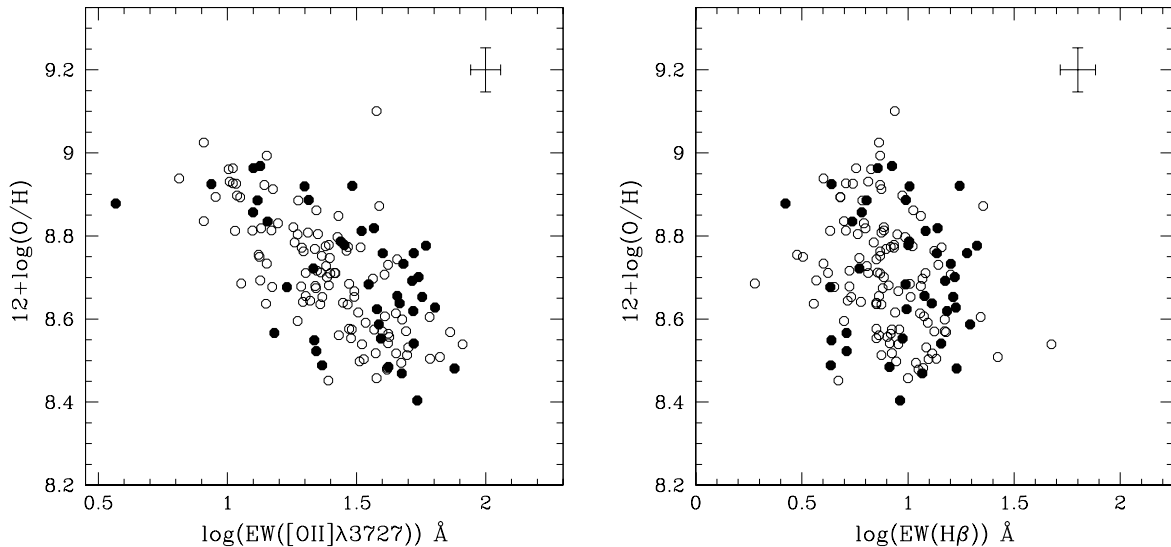


**Figure 10.** Relationship between oxygen abundance in terms of  $12 + \log(\text{O}/\text{H})$ , estimated using  $R_{23}$  parameter and assuming that all star-forming galaxies lie on the upper branch of  $R_{23}$  vs.  $12 + \log(\text{O}/\text{H})$  calibration, and rest-frame  $[\text{OII}]\lambda 3727$  (left panel) and  $\text{H}\beta$  (right panel) emission line equivalent widths. Intermediate redshift star-forming galaxies are shown as filled circles, and the NFGS sample of local star-forming galaxies is marked by open circles.

Extensive studies have been dedicated to calibrating the relation between  $R_{23}$  and oxygen abundance (e.g., McCall et al. 1985; Pilyugin 2001), and now strong-line ratios can reliably indicate the oxygen abundance to within the accuracy of the model calibrations, approximately  $\pm 0.15$  dex. The  $R_{23}$  parameter is both abundance- and ionization-sensitive (e.g., Kewley & Dopita 2002). The correction of this dependence of  $R_{23}$  parameter on ionization is usually done by using the ionization-sensitive diagnostic ratio

$\text{O}_{32} = [\text{OIII}]\lambda 4959, \lambda 5007 / [\text{OII}]\lambda 3727$  (e.g., McGaugh 1991; Kewley & Dopita 2002). Generally, the  $[\text{OIII}]\lambda 4959$  emission line is of a low signal-to-noise. We thus use the theoretical ratio  $[\text{OIII}]\lambda 5007 / [\text{OIII}]\lambda 4959 = 3$  to estimate the  $[\text{OIII}]\lambda 4959$  equivalent width (Osterbrock 1989).

The galaxy spectra analysed here are not flux-calibrated, so we use emission line equivalent widths to estimate both the  $R_{23}$  and  $\text{O}_{32}$  parameters. We follow the prescription of Kobulnicky & Phillips (2003) for estimat-

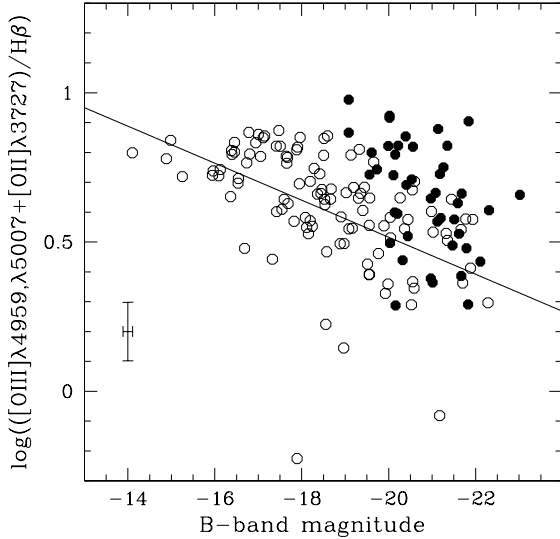


**Figure 6.** The metallicity-sensitive  $([\text{OIII}]\lambda 4959, \lambda 5007 + [\text{OII}]\lambda 3727)/\text{H}\beta$  ratio versus  $M_B$  diagram for the sample considered in the paper, shown as filled circles, and the local comparison sample of star-forming galaxies, shown as open circles. The solid line is the fit of Jansen et al. (2001). A fraction of luminous (and massive) star-forming galaxies at intermediate redshift show large  $([\text{OIII}]\lambda 4959, \lambda 5007 + [\text{OII}]\lambda 3727)/\text{H}\beta$  ratios indicative of low oxygen abundances.

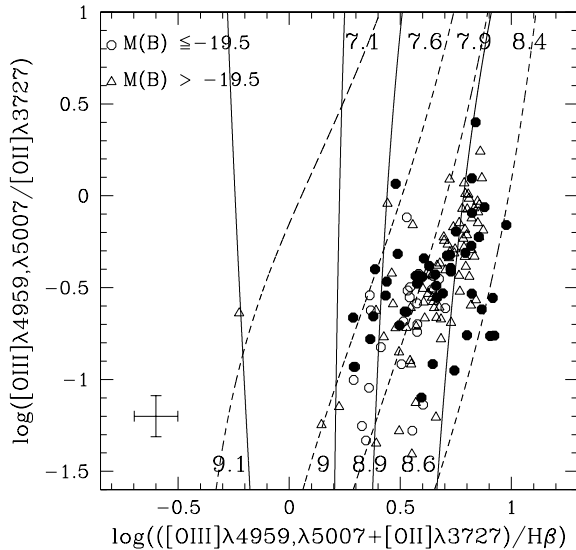


**Figure 7.** The  $([\text{OIII}]\lambda 4959, \lambda 5007 + [\text{OII}]\lambda 3727)/\text{H}\beta$  versus  $[\text{OIII}]\lambda 4959, \lambda 5007 / [\text{OII}]\lambda 3727$  diagram for the sample considered in this paper. Also shown is the McGaugh (1991) calibration of tracks with constant metallicity. Models with oxygen abundances lower than  $12 + \log(\text{O}/\text{H}) \lesssim 8.4$  are shown as dashed lines, those with higher oxygen abundances are shown by continuous lines. Symbols are the same as in the right panel of Fig. 5.

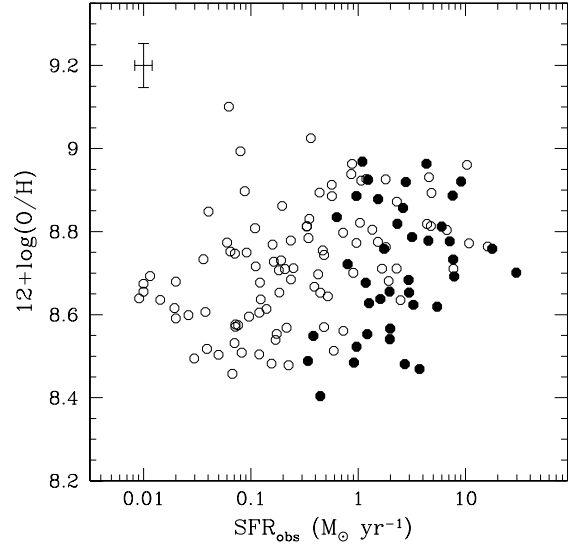


**Figure 11.** Relationship between oxygen abundance in terms of  $12 + \log(\text{O}/\text{H})$  and observed star formation rate for the sample of intermediate redshift star-forming galaxies (filled circles), and the NFGS sample of local star-forming galaxies (open circles). The current star formation rate has been estimated for our galaxy sample using  $\text{H}\beta$  emission line luminosity corrected for stellar absorption, but not for internal dust obscuration, and using extinction-uncorrected  $\text{H}\alpha$  luminosity for the NFGS sample.

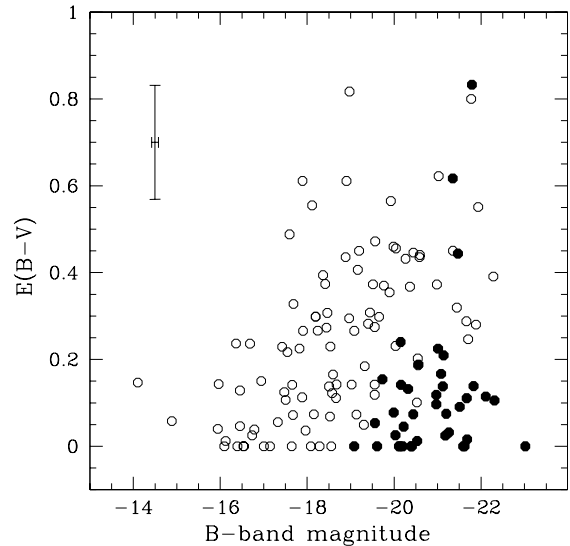


**Figure 12.** Relationship between colour excess and B-band magnitude for the sample of intermediate redshift field galaxies (filled circles), and the NFGS sample of local star-forming galaxies (open circles). No correlation is observed for intermediate redshift star-forming galaxies.

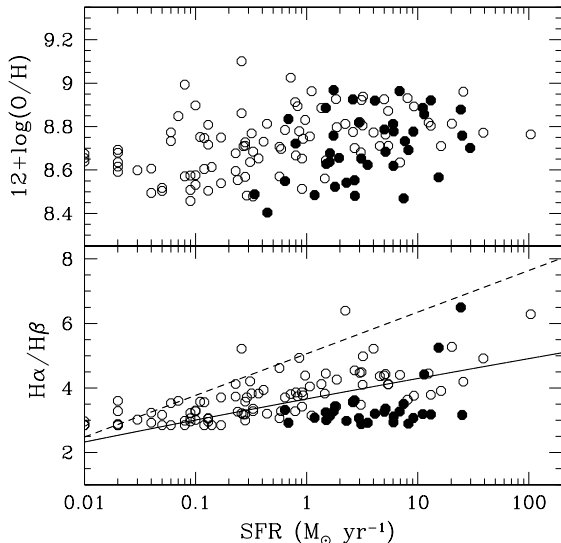


**Figure 13.** Upper panel: the relationship between oxygen abundance and extinction-corrected star formation rate for the sample of intermediate redshift star-forming galaxies (filled circles), and the local sample of star-forming galaxies from the NFGS sample (open circles). Lower panel: the relationship between Balmer decrement and extinction-corrected star formation rate. Symbols are the same as for the upper panel. The solid line represents the relationship derived by Hopkins et al. (2001) for a sample of local star-forming galaxies, while the dashed line indicates the relationship for a sample of radio-selected galaxies from Afonso et al. (2003).

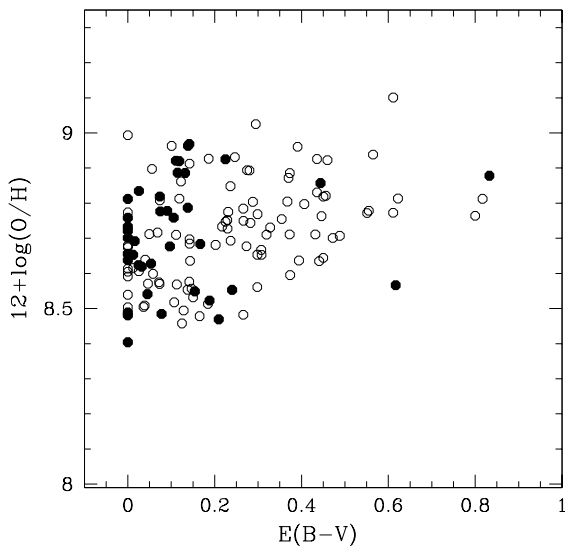


**Figure 14.** Relationship between gas phase oxygen abundance and colour excess for the sample of intermediate redshift star-forming galaxies (filled circles), and the local sample of star-forming galaxies from the NFGS sample (open circles).

ing the gas phase oxygen abundances using strong emission line equivalent widths. Further analysis using flux-calibrated spectra of both local and intermediate redshift galaxies have shown that, for a large range of nebular reddening,  $R_{23}$ -based oxygen abundances and ionization-sensitive ratios based on emission line equivalent widths offer comparable precision to estimates using reddening-corrected fluxes (see Moustakas & Kennicutt 2006 and Lamareille et al. 2006 for more details). This suggests that  $R_{23}$  and  $O_{32}$  parameters are not significantly affected by the differential reddening between the stars and the emitting gas.

The strong line method has been suspected to involve systematic errors, being biased toward higher values of oxygen abundances than the method based on temperature-sensitive auroral lines, especially at the high-metallicity end (Kennicutt et al. 2003). The debate over whether the discrepancies in the abundance scales are due to systematic biases in the electronic temperature-based scale, or in the HII region models used to calibrate different strong-line vs. abundance relations, particularly in the high-metallicity regime, is not yet settled. Note that the oxygen abundance estimated using different calibrations available in the literature might differ by factors of up to  $\sim 4$  (Ellison & Kewley 2005). However, as our main interest is to study the relative change in oxygen abundance between star-forming galaxies at the present epoch and those at intermediate redshifts, the exact choice of the  $12 + \log(O/H)$  versus  $R_{23}$  calibration is not a critical issue. Here we determine oxygen abundance using the calibration of McGaugh (1991), as found in Kobulnicky, Kennicutt & Pizagno (1999).

Fig. 7 shows the relationship between  $R_{23}$  parameter and  $[OIII]\lambda 4959, \lambda 5007/[OII]\lambda 3727$  ratio for star-forming galaxies in both the local NFGS sample, and at intermediate redshifts. To show the effect of galaxy luminosity, we split the local sample of star-forming galaxies into faint ( $M_B > -19.5$ ) and bright ( $M_B \leq -19.5$ ) subsamples. The McGaugh (1991) calibration of the relationship between  $R_{23}$  and  $[OIII]\lambda 4959, \lambda 5007/[OII]\lambda 3727$  is overplotted. Different lines show this relationship for different oxygen abundances, in terms of  $12 + \log(O/H)$ . The figure shows that star-forming galaxies in both the local and intermediate redshift samples are distributed similarly in the  $R_{23}$  parameter versus  $[OIII]\lambda 4959, \lambda 5007/[OII]\lambda 3727$  ratio diagram. As shown in the previous section, a fraction of luminous intermediate redshift field galaxies are located in a similar area as faint local star-forming galaxies with intermediate ionization-sensitive  $[OIII]\lambda 4959, \lambda 5007/[OII]\lambda 3727$  ratios and  $R_{23}$  parameter. Similar to what is found by Lilly et al. (2003) for a  $H\beta$ -selected galaxy sample and Liang et al. (2004) for a sample of luminous infrared galaxies, none of the intermediate redshift galaxies in our sample show a  $[OIII]\lambda 4959, \lambda 5007/[OII]\lambda 3727$  ratio significantly larger than unity, as observed for some extragalactic HII regions in nearby galaxies (e.g., van Zee et al. 1998) and a few  $z \gtrsim 2$  luminous galaxies (Kobulnicky & Koo 2000, Pettini et al. 2001, Lemoine-Busserolle et al. 2003). The sample of intermediate redshift star-forming galaxies studied by Maier et al. (2004) does contain a few galaxies with  $[OIII]\lambda 4959, \lambda 5007/[OII]\lambda 3727$  larger than unity. However, all these intermediate redshift highly ionized galaxies are 2–3 magnitudes fainter than the galaxies in our sample.

A well-known complication of the use of  $R_{23}$  to estimate

the oxygen abundance is that the dependency on metallicity of this parameter is degenerate. Indeed, at a fixed value of  $R_{23}$  two different values of metallicity are possible: at the same oxygen abundance, different ionization parameters lead to different values of  $R_{23}$  (McCall et al. 1985).  $R_{23}$  increases with oxygen abundance in the low-metallicity regime ( $12 + \log(\text{O}/\text{H}) \lesssim 8.2$ ; in this scale the solar value is 8.69; Allende Prieto et al. 2001), while for metal-rich objects ( $12 + \log(\text{O}/\text{H}) \gtrsim 8.4$ ) it decreases with  $\text{O}/\text{H}$ , reflecting the efficiency of oxygen cooling over abundance in these objects. In the “intermediate” metallicity region ( $8.2 \lesssim 12 + \log(\text{O}/\text{H}) \lesssim 8.4$ ), galaxies may have a large range of metallicities for a narrow range of  $R_{23}$ . The uncertainties in this metallicity domain, i.e. whether an object with a given  $R_{23}$  parameter lies on the metal-rich branch or on the metal-poor branch of the  $12 + \log(\text{O}/\text{H})$  vs.  $R_{23}$  relation, dominate the uncertainties related to model calibrations.

A variety of abundance indicators have been used to break the degeneracy, e.g.  $[\text{NII}]\lambda 6584/[\text{OIII}]\lambda 4959$  (Alloin et al. 1979),  $[\text{NII}]\lambda 6584/[\text{OII}]\lambda 3727$  (McGaugh 1994),  $[\text{NII}]\lambda 6584/\text{H}\alpha$  (van Zee et al. 1998, Denicoló et al. 2002). Unfortunately, the data available is not enough to break the  $R_{23}$  degeneracy, i.e., none cover the  $\text{H}\alpha$  and  $[\text{NII}]\lambda 6584$  spectral range. However, the majority of intermediate redshift star-forming galaxies with  $M_B \lesssim -20$ , for which the  $R_{23}$ -metallicity degeneracy has been broken, are found to lie on the metal-rich branch of the  $12 + \log(\text{O}/\text{H})$  versus  $R_{23}$  calibration (Kobulnicky et al. 2003; Lilly et al. 2003; Kobulnicky & Kewley 2004, Maier et al. 2005). While the exact location of galaxies in our sample on the  $12 + \log(\text{O}/\text{H})$  versus  $R_{23}$  calibration cannot be determined reliably until near-infrared spectroscopy is available for our sample galaxies, we make the reasonable assumption that the luminous star-forming galaxies in our sample lie on the upper metallicity branch of the  $12 + \log(\text{O}/\text{H})$  versus  $R_{23}$  calibration. The expected oxygen abundances of intermediate redshift massive galaxies in the case where they lie on the lower metallicity branch are extremely low, suggesting improbably large evolutionary changes in the metallicities of massive galaxies between  $z \sim 0.5$ – $1.0$  and the present epoch (see Lilly et al. 2003; Ellison et al. 2005).

For four galaxies in our sample, the oxygen abundance estimated using the low-branch of metallicity calibration was larger than the one derived using the upper-branch of the metallicity calibration. These galaxies have been excluded from the sample. This may happen when the  $R_{23}$  is larger than the maximum value predicted by the model grid used to calibrate the relation between  $12 + \log(\text{O}/\text{H})$  and  $R_{23}$ . The eighth column of Table 2 lists the estimated oxygen abundances.

Fig. 8 shows the relationship between galaxy B-band absolute magnitude and oxygen abundance in terms of  $12 + \log(\text{O}/\text{H})$  for our sample of intermediate redshift star-forming galaxies compared with several other samples. The comparison samples are the local relation defined by star-forming galaxies from the NFGS sample, and three intermediate redshift samples for which the gas-phase oxygen abundances were estimated using the strong emission line method, similar to our procedure. These are: the  $\text{H}\beta$ -selected sample of Lilly et al. (2003), a sample of star-forming galaxies drawn from the Deep Extragalactic Evolutionary Probe Survey of Groth Strip galaxies (Kobulnicky et al. 2003), and

the sample of intermediate redshift luminous infrared galaxies of Liang et al. (2004). All star-forming galaxies in the NFGS sample are assumed to lie on the upper metallicity branch of the  $12 + \log(\text{O}/\text{H})$  vs.  $R_{23}$  calibration, as was assumed for the intermediate redshift galaxy samples. As expected from the comparison of different diagnostic ratios observed for our sample galaxies with what is seen for local star-forming galaxies with known oxygen abundances (see section 3.3), the estimated oxygen abundances for galaxies in our sample cover a large range, i.e.,  $8.4 \lesssim 12 + \log(\text{O}/\text{H}) \lesssim 9$ , similar to that seen for star-forming galaxies in the NFGS sample, with a mean of 8.7.

The upper-left panel of Fig. 8 shows the well-established correlation between luminosity and oxygen abundance for galaxies in the local universe (e.g., Melbourne & Salzer 2002; Lamareille et al. 2004; Tremonti et al. 2004), with a large scatter, however, which could be related to the variety of star formation histories in these galaxies (see e.g., Mouhcine & Contini 2002). Unlike local galaxies, a clear correlation between galaxy luminosity and oxygen abundance is not observed for our sample of star-forming field galaxies at intermediate redshifts. Rather, a broad range of oxygen abundances of the interstellar star-forming gas at any given galaxy luminosity is observed. Our sample contains luminous galaxies that exhibit oxygen abundances similar to those seen for bright galaxies at the present epoch, i.e.,  $12 + \log(\text{O}/\text{H}) \sim 8.8$ – $9$ , suggesting that the chemical properties of this population of intermediate redshift galaxies will not evolve significantly to the present epoch. This is in agreement with recent studies of the chemistry of luminous star-forming galaxies at intermediate redshifts (e.g., Kobulnicky & Kewley 2004).

However, a subsample of luminous intermediate redshift star-forming galaxies show oxygen abundances lower than what is observed for local galaxies with similar luminosities, i.e.,  $12 + \log(\text{O}/\text{H}) \sim 8.4$ – $8.6$ , in agreement with the recent finding of Maier et al. (2005). Given their rotation velocities and physical sizes, the population of metal-poor galaxies in our sample is likely to evolve into massive metal-rich galaxies in the local universe. Their evolution in the luminosity vs. metallicity diagram will be vertical rather than horizontal. Thus, these galaxies are on the process of building up their metal content. This is in agreement with the suggested scenario of Lilly et al. (2003), who argue based on galaxy properties, i.e., optical and near-infrared photometry, morphological properties and oxygen abundances, that bright intermediate redshift galaxies with intermediate oxygen abundances are likely to evolve into metal-rich disk galaxies at the present epoch by a progressive enrichment of their metal content, rather than fade into local dwarf galaxies. The appearance of a population of luminous and metal-poor galaxies at intermediate redshifts should affect the luminosity-metallicity relation at this redshift range, in the sense that galaxies of a given luminosity become, on average, more metal-poor at higher redshift (see e.g., Kobulnicky & Kewley 2004).

The upper-right panel of Fig. 8 compares the luminosity-metallicity relation of our sample of intermediate redshift galaxies with the sample of galaxies from Kobulnicky et al. (2003), with  $0.26 < z < 0.82$ . Note that Kobulnicky et al. (2003) used emission line equivalent widths rather than fluxes to estimate oxygen abundances, similar

to our procedure. The oxygen abundances of both samples cover similar ranges, however the sample of Kobulnicky et al. (2003) extends to fainter luminosities. Unlike our sample galaxies, the intermediate redshift galaxy sample from Kobulnicky et al. (2003) shows a trend between galaxy luminosity and gas phase oxygen abundance. Galaxies in our intermediate redshift sample cover a wider range of oxygen abundance at a given luminosity. Overall the Kobulnicky et al. (2003) galaxies tend to be fainter at a given oxygen abundance. However, this difference simply reflects that our sample is limited to brighter galaxies than the rest-frame B-band selected sample from which the Kobulnicky et al. (2003) sample has been drawn (see also Liang et al. 2004).

The lower-left panel of Fig. 8 compares the luminosity–metallicity relation of our intermediate redshift star-forming galaxies with a sample of Canada-France Redshift Survey galaxies with  $0.47 < z < 0.92$  from Lilly et al. (2003). Both samples show similar luminosity–metallicity relations.

Liang et al. (2004) investigated the luminosity–metallicity relation for a sample of intermediate redshift, luminous infrared ( $15\mu\text{m}$ -selected) galaxies with  $0.4 < z < 1.16$ . The comparison between the luminosity–metallicity relation for our sample galaxies and the sample of luminous infrared galaxies of Liang et al. (2004) is shown in the lower-right panel of Fig. 8. Interestingly, both galaxy samples show similar relations, despite the fact that optically selected galaxy samples and mid-infrared selected galaxy samples tend to select different population of galaxies, i.e., luminous infrared galaxies in the Liang et al. (2004) sample tend to show on average larger internal dust obscuration and intrinsic star formation rates than galaxies in our sample (see Section 4.2 for a discussion of the distribution of the star formation rate and colour excess for the galaxies in our sample). The similarity of the observed luminosity–metallicity relations might be due to that luminous infrared galaxies at intermediate redshifts showing similar rest-frame optical and spectral properties to normal starburst galaxies, and suggests the differences in the selection procedure do not lead to a significant bias against a given class of galaxies (Hammer et al. 2005).

If the assembly of galaxy stellar mass, and subsequently its metal content, is related to the size of the dark matter halo where a galaxy sits, the degree of the interstellar gas chemical evolution is expected to correlate with maximum rotation velocity of the halo. Fig. 9 shows the relations between oxygen abundance in terms of  $12 + \log(\text{O}/\text{H})$  and rotation velocity and emission length scale, shown in the left and right panels, respectively, for our sample of star-forming field galaxies. No convincing correlations are seen between gas phase oxygen abundance and rotation velocity or emission length scale. For a given rotation velocity or galaxy size, intermediate redshift galaxies exhibit a wide range of gas phase oxygen abundances. This is consistent with the lack of a correlation between gas phase oxygen abundance of luminous intermediate redshift star-forming galaxies and their I-band half-light radius reported by Lilly et al. (2003). This contrasts however with the reported positive trend between gas phase oxygen abundance and rotation velocity for local spiral galaxies (Zaritsky et al. 1994). This suggests that at least a fraction of massive and large galaxies at intermediate redshifts continue the assembly of their chemical content after  $z \sim 1$ . Metal-rich and metal-poor galaxies cover sim-

ilar ranges of rotation velocity and physical size, implying that both galaxy populations reside within similar halos, and that the size of the halo is not the only parameter that affects galactic chemical enrichment history.

## 4.2 Star formation and dust obscuration

The population of luminous field galaxies at intermediate redshifts consists of a mixture of galaxies with different levels of chemical evolution and interstellar gas properties. This suggests that intermediate redshift luminous galaxies might have a variety of star formation histories, and thus could exhibit further differences in their intrinsic properties.

Fig. 10 shows the relationship between oxygen abundance in terms of  $12 + \log(\text{O}/\text{H})$  and rest-frame equivalent width of the  $[\text{OII}]\lambda 3727$  and  $\text{H}\beta$  emission lines respectively. A clear correlation is visible between gas phase oxygen abundance and  $[\text{OII}]\lambda 3727$  emission line rest-frame equivalent width. However, no convincing trend is observed between oxygen abundance and  $\text{H}\beta$  emission line rest-frame equivalent width as also seen by Lilly et al. (2003) and Kobulnicky et al. (2003). This could be due to an unreliable correction of the underlying stellar Balmer lines in absorption which might introduce an extra scatter to the relation.

Emission line equivalent widths can be considered as rough tracers of the current relative star formation, in the sense of absolute current star formation rate relative to the total integrated star formation rate, i.e., the star formation rate per unit luminosity. Intermediate redshift and local star-forming galaxies are distributed similarly in oxygen abundance vs. emission line rest-frame equivalent width diagrams, suggesting that massive, metal-poor field galaxies at intermediate redshifts might have similar relative star formation histories to local faint and metal-poor star-forming galaxies. The observed trend might be taken to suggest that systems with low metallicities on average show higher relative star formation rates than metal-rich galaxies. The absence of a correlation between oxygen abundance and rotation velocity suggests that this might be the case independent of the size of the galaxy halo.

Fig. 11 shows the relationship between oxygen abundance and star formation rate for star-forming galaxies in both the local NFGS comparison galaxy sample, shown as open circles, and our galaxy sample, shown as filled circles. The star formation rates of intermediate redshift galaxies are derived using  $\text{H}\beta$  luminosities, estimated using  $\text{H}\beta$  equivalent widths and B-band absolute luminosities as given by equation 6 of Kobulnicky & Kewley (2004). The star formation rates are then calculated following the calibration of Kennicutt (1998). The estimated star formation rates, in solar masses per year, are listed in the 9th column of Table 2.  $\text{H}\beta$  emission line luminosities were not corrected for internal reddening, thus the estimated star formation rates of intermediate redshift galaxies must be considered as lower limits. The star formation rate of star-forming galaxies in the NFGS sample has been estimated using extinction-uncorrected  $\text{H}\alpha$  luminosity following the calibration of Kennicutt (1998).

Local star-forming galaxies exhibit a correlation between oxygen abundance of the interstellar gas and the extinction-uncorrected star formation rate, in the sense of higher oxygen abundances for galaxies with higher observed star formation rate, i.e., observed  $\text{H}\alpha$  luminosity. However,

no clear trend is obvious for intermediate redshift galaxies: metal-poor and metal-rich luminous star-forming galaxies cover a similar range of extinction-uncorrected star formation rate. Metal-rich luminous star-forming galaxies at intermediate redshifts show, at a given oxygen abundance, similar extinction-uncorrected star formation rates to their local counterparts. This could be the case if metal-rich luminous galaxies at intermediate redshift are affected by a similar amount of internal dust obscuration as their counterparts at the present epoch. Alternatively, this could be the case if they show, at a given gas phase oxygen abundance, higher/lower Balmer intrinsic emission line fluxes and lower/higher internal reddening than metal-rich star-forming galaxies locally. On the other hand, metal-poor luminous galaxies at intermediate redshift show on average larger extinction-uncorrected star formation rates than local galaxies with similar gas phase oxygen abundances. This might be due to that metal-poor galaxies at intermediate redshift have higher intrinsic star formation rates or lower internal reddening than their local counterparts. To distinguish between these possibilities, internal dust obscuration affecting intermediate redshift star-forming galaxies should be estimated.

As mentioned earlier, none of the objects in our sample have both  $H\alpha$  and  $H\beta$  emission line present in their covered spectral range, so the dust obscuration cannot be derived using the Balmer decrement. However, by comparing the energy balance between the luminosities of two different star formation indicators that are free from systematic effects other than dust reddening, i.e., that do not depend on metallicity or excitation state of the emitting gas, it is possible to estimate the amount of internal extinction affecting a galaxy's spectrum. Using  $H\beta$  and  $[\text{OII}]\lambda 3727$  emission lines as star formation rate indicators, the colour excess can be estimated using the relation:

$$E(B - V) = \frac{2.5}{\kappa(H\beta) - \kappa(\text{OII})} \log \left( \frac{\text{SFR}(\text{OII})_{\text{obs}}}{\text{SFR}(H\beta)_{\text{obs}}} \right) \quad (4)$$

where  $\kappa(\lambda)$  is the optical interstellar extinction curve. We adopt the Milky Way interstellar extinction law of Cardelli, Clayton, & Mathis (1989), with  $R_V = 3.1$ . The  $[\text{OII}]\lambda 3727$  emission line is a widely used star formation indicator for galaxies at the redshift range where the  $H\alpha$  emission line moves into the near-infrared (e.g., Thompson & Djorgovski 1991; Cowie et al. 1997; Hogg et al. 1998; Hippelein et al. 2003). However, published calibrations of the star formation rate in terms of  $[\text{OII}]\lambda 3727$  vary by factors of a few (Gallagher et al. 1989; Kennicutt 1992; Guzmán et al. 1997; Rosa-González et al. 2002). The  $[\text{OII}]\lambda 3727$  emission line shows a complex behaviour as a function of galaxy and interstellar gas properties. Locally, for star-forming galaxies with ionization-sensitive  $[\text{OIII}]\lambda 4959, \lambda 5007 / [\text{OII}]\lambda 3727$  ratios similar to what is observed for the intermediate redshift galaxies studied in this paper, and with  $12 + \log(\text{O}/\text{H}) \gtrsim 8.4$ , the variation of observed  $[\text{OII}]\lambda 3727 / H\alpha$  flux ratio is regulated by extinction and metallicity, with no sizeable sensitivity to the excitation state of the ionized gas (Kewley et al. 2004; Mouhcine et al. 2005). The star formation rate in terms of the  $[\text{OII}]\lambda 3727$  emission line is estimated using the calibration:

$$\text{SFR}(\text{M}_\odot \text{yr}^{-1}) = 7.9 \times 10^{-42} L_{[\text{OII}]}(\text{erg s}^{-1}) \times f(\text{O}/\text{H}) \quad (5)$$

where  $L_{[\text{OII}]}$  is the observed  $[\text{OII}]\lambda 3727$  luminosity, and  $f(\text{O}/\text{H})$  is a correction factor introduced by Kewley et al. (2004) to account for the effect of metallicity on the variation of  $[\text{OII}]\lambda 3727 / H\alpha$  flux ratio, i.e.,  $f(\text{O}/\text{H}) = 1 / [-2.29 + 21.21 \times (12 + \log(\text{O}/\text{H}))]$  (see Kewley et al. 2004).

The  $[\text{OII}]\lambda 3727$  emission line luminosity is estimated from the equivalent width ( $W([\text{OII}])$ ) and the rest-frame absolute  $B$ -band magnitude. For this we estimate the continuum flux at the position of the  $[\text{OII}]$  line from  $M_B$  and the spectral energy distribution which best fits the available colours, which was used to determine  $M_B$  from the observed magnitudes in the first place. The absolute continuum flux at the effective wavelength of the  $B$ -band ( $\sim 4450\text{\AA}$ ) was calculated from the rest-frame absolute  $B$ -band magnitudes using the conversion given by Fukugita et al. (1995)  $F_{\text{cont},B} = 6.19 \cdot 10^{-9} \cdot 10^{-0.4M_B} \text{ erg s}^{-1} \text{ cm}^{-2} \text{ \AA}^{-1}$ . Using the spectral energy distributions of Aragón-Salamanca et al. (1993), which were used in the determination of the VLT  $M_B$  and are similar in the range of interest to those used for the Subaru  $M_B$  (Fukugita et al. 1995), the ratios of the continuum flux at  $[\text{OII}]\lambda 3727$  ( $F_{\text{cont},[\text{OII}]}$ ) to that at the  $B$ -band effective wavelength ( $F_{\text{cont},B}$ ) are 0.45, 0.53, 0.67, 0.74, and 0.83 for types E/S0, Sab, Sbc, Scd, and Sdm respectively (Milvang-Jensen 2003). An approximate conversion was used to convert the types used for the Subaru data onto the system used for the VLT data. The ratio was interpolated between the listed values for intermediate types. The absolute flux in the  $[\text{OII}]\lambda 3727$  line is then simply  $F_{[\text{OII}]} = W([\text{OII}]) \cdot F_{\text{cont},[\text{OII}]}$ .

Since a negative colour excess is unphysical, we assume that galaxy properties that give rise to  $E(B - V) < 0$  correspond to zero attenuation. The estimated colour excess for our intermediate redshift star-forming galaxies are listed in the last column of Table 2.

Fig. 12 shows the relationship between the colour excess and galaxy luminosity for star-forming galaxies in both the local comparative sample, and the intermediate redshift sample. No correlation is found between galaxy luminosity and nebular extinction for intermediate redshift galaxies, in agreement with the finding of Maier et al. (2005). The estimated colour excesses for intermediate redshift galaxies are distributed over a range similar to that seen across a large sample of local star-forming galaxies with  $-14.0 \lesssim M_B \lesssim -22.0$ . However, the mean colour excess for intermediate redshift galaxies in our sample, i.e.,  $0.16 \pm 0.03$  when excluding galaxies with  $E(B - V) = 0$  and  $0.12 \pm 0.03$  when all galaxies are included, is significantly lower than the observed average colour excess,  $E(B - V) \sim 0.3$ , for local star-forming galaxies (e.g., Nakamura et al. 2004, Hopkins et al. 2003, Kewley et al. 2004, Mouhcine et al. 2005). Star-forming galaxies at intermediate redshifts show a larger scatter of colour excess at a given galaxy luminosity than observed locally: a fraction of luminous star-forming galaxies at intermediate redshifts show amounts of dust obscuration similar to what is observed for their local counterparts, while another subpopulation of luminous galaxies show dust obscuration similar to that observed locally for fainter galaxies.

The comparison of different star formation rate indicators for local samples of star-forming galaxies, selected at optical or ultra-violet wavelengths, have shown a clear trend for increasing dust obscuration with intrinsic star formation rate (e.g., Wang & Heckman 1996; Sullivan et al. 2001; Buat

et al. 2002). The lower panel of Fig.13 shows the relationship between the Balmer decrement, estimated using the derived  $E(B-V)$  and the extinction curve of Cardelli et al. (1989), and the extinction-corrected star formation rate for the local comparative sample, shown as open circles, and our sample of star-forming field galaxies. The solid line shows the relationship derived from Hopkins et al. (2001) for a sample of local galaxies, while the dotted line indicates the relationship for a radio-selected sample of star-forming galaxies to  $z \approx 0.8$  from Afonso et al. (2003). The distribution of local star forming galaxies in the NGFS sample agrees nicely with the relationship from Hopkins et al. (2001), however they deviate significantly from the relationship observed for radio-selected galaxies. This could be because radio-selected galaxy samples tend to be biased toward dustier galaxies than optically selected samples. The star-forming galaxies in our intermediate redshift galaxy sample deviate systematically, especially those with star formation rates lower than  $\sim 10M_{\odot}\text{yr}^{-1}$ , from the fit of Hopkins et al. (2001), indicating that for a given star formation rate, star-forming galaxies at earlier cosmic epochs show on average lower internal reddening than their local counterparts. Galaxies with star formation rate larger than  $\sim 10M_{\odot}\text{yr}^{-1}$  display Balmer decrements and a scatter similar to what is observed for local star-forming galaxies.

The upper panel of Fig.13 shows the relationship between gas phase oxygen abundance and extinction-corrected star formation rate for the local comparative sample and the sample of intermediate redshift star-forming galaxies. The trend observed locally between oxygen abundance and extinction-uncorrected star formation rate (see Fig.11) is still visible after the extinction correction of the star formation rate. A similar trend has also been observed recently for a sample of blue compact galaxies (Kong 2004). No convincing trend is observed for star-forming galaxies in our intermediate redshift sample. Metal-poor luminous galaxies at intermediate redshifts show higher extinction-corrected star formation rates than observed locally for galaxies with similar oxygen abundances, while metal-rich luminous galaxies show extinction-corrected star formation rates similar to those observed for their local counterparts in agreement with what was reported recently for a sample of Canada-France Redshift Survey galaxies (Maier et al. 2005).

There have been contradictory claims regarding a possible correlation between dust obscuration and metallicity of galaxies in the local universe. Zaritsky et al. (1994) have reported no clear evidence for a sensitivity of internal reddening to abundance in a sample of disk galaxies, suggesting that abundance and extinction are not necessarily linked. It has been found, however, for other local galaxy samples that the extinction derived from the Balmer decrement correlates with metallicity (e.g., Stasińska & Sodre 2001; Kong et al. 2002). The observed trends between galaxy luminosity, metallicity, dust extinction, and star formation rate for local star-forming galaxies, suggest that the main driver of the extinction of galaxies is their mass, combined with their metallicity (and probably the presence of old stellar populations; Stasińska et al. 2004). Fig.14 shows the relationship between gas phase oxygen abundance and colour excess for the local comparison sample and our sample of intermediate redshift galaxies. Locally, a positive trend is apparent between oxygen abundance and colour excess, although

with a large scatter (see Stasińska & Sodré 2001; Kewley et al. 2004 who analysed the properties of the same local galaxy sample). Strikingly, luminous star-forming galaxies in our intermediate redshift sample and local star-forming galaxies in the NGFS sample distribute similarly in the oxygen abundance vs. colour excess diagram. Combining this with the absence of a correlation between galaxy luminosity and colour excess for intermediate redshift luminous star-forming galaxies, one might conclude that the dust obscuration is primarily a function of the level of galaxy chemical enrichment rather than luminosity. This emphasizes the importance of accurate estimates of dust obscuration, using Balmer decrements or the energy balance between different observed star-formation indicators, to determine the oxygen abundances properly (see also Maier et al. 2005). Consequently, the evolution of the luminosity–metallicity relation as a function of cosmic epoch implies that one cannot use the local relationship between galaxy luminosity and colour excess to estimate the dust obscuration affecting galaxies at earlier cosmic epochs based only on their luminosities.

## 5 DISCUSSION

We have thus found that the properties of the interstellar star-forming gas in massive and large field galaxies at intermediate redshifts cover a wide range, extending from those observed for local bright metal-rich galaxies, i.e., weak emission lines, low ionization conditions, high oxygen abundances and high dust obscuration, to those of local metal-poor dwarf galaxies which exhibit signatures of strong ongoing star-formation activity, i.e., strong emission lines, high ionization conditions, low oxygen abundances, and low dust obscuration.

A fraction of massive field galaxies at intermediate redshifts have already undergone a significant chemical enrichment, as indicated by their high oxygen abundances. This suggests that this population of galaxies have already formed a large fraction of the stellar mass observed at the present epoch in massive, metal-rich galaxies. This is consistent with the reported mild evolution of the galaxy stellar mass function of the massive galaxy population since  $z \sim 1$ , implying that the evolution of these galaxies is essentially complete by this redshift (e.g., Brinchmann & Ellis 2000, Fontana et al. 2004, Drory et al. 2004, Bundy et al. 2005). The relationship between stellar mass and maximum rotation velocity, i.e., the baryonic Tully-Fisher relation, out to  $z \sim 1$  seems to be largely consistent with the local relation (Conselice et al. 2005; but see Flores et al. 2005 for a different view). These observational constraints are consistent with the downsizing picture for galaxy evolution. In this scenario, introduced initially by Cowie et al. (1996), the mass threshold below which star-forming galaxies, defined as galaxies in which the formation timescale is less than the Hubble time at the galaxy redshifts, are found, decreases with cosmic epoch. Consequently, the star formation activity, and hence chemical evolution, seems to stop within the highest mass galaxies at earlier cosmic epochs than for less massive galaxies (see also Fig. 5 of Maier et al. 2006).

On the other hand, a sub-population of massive and luminous intermediate redshift star-forming galaxies, with emission length sizes larger than 2 kpc, appear to be at ear-

**Table 2.** Properties of our sample of intermediate redshift field galaxies. The columns give the ID, redshift, absolute rest-frame  $B$ -band magnitude, rest-frame rotation velocity, emission scalelength, star formation rate determined from  $H\beta$ , and the colour excess due to internal dust extinction, respectively.

ID	$z$	$M_B$ mag	EW([OII] $\lambda$ 3727) ( $\text{\AA}$ )	EW( $H\beta$ ) ( $\text{\AA}$ )	EW([OIII] $\lambda$ 5007) ( $\text{\AA}$ )	$V_{rot}$ (kms $^{-1}$ ) (kms $^{-1}$ )	size (kpc) (kpc)	12 + log(O/H)	SFR( $M_\odot$ yr $^{-1}$ ) ( $M_\odot$ yr $^{-1}$ )	E(B-V) (mag)
1	0.547	-21.47 $\pm$ 0.11	12.57 $\pm$ 1.67	6.06 $\pm$ 0.97	4.67 $\pm$ 0.77	234.86 $\pm$ 37.75	5.18 $\pm$ 0.57	8.86 $\pm$ 0.06	2.62 $\pm$ 0.42	0.44 $\pm$ 0.25
2	0.305	-21.01 $\pm$ 0.19	8.66 $\pm$ 0.87	4.36 $\pm$ 0.28	1.11 $\pm$ 0.19	98.12 $^{+40.91}_{-17.42}$	3.67 $\pm$ 0.63	8.93 $\pm$ 0.02	1.24 $\pm$ 0.08	0.23 $\pm$ 0.13
3	0.325	-19.08 $\pm$ 0.17	54.38 $\pm$ 4.09	9.18 $\pm$ 0.99	10.07 $\pm$ 0.98	99.02 $\pm$ 11.5	3.43 $\pm$ 0.15	8.40 $\pm$ 0.15	0.44 $\pm$ 0.05	0.000 $\pm$ 0.22
4	0.682	-21.59 $\pm$ 0.04	47.99 $\pm$ 2.24	15.92 $\pm$ 1.04	15.31 $\pm$ 1.60	...	...	8.73 $\pm$ 0.05	7.68 $\pm$ 0.50	0.000 $\pm$ 0.12
5	0.346	-20.97 $\pm$ 0.15	16.99 $\pm$ 1.81	4.31 $\pm$ 0.8	1.59 $\pm$ 0.64	181.59 $^{-18.71}_{+14.34}$	16.1 $^{-0.35}_{+1.87}$	8.68 $\pm$ 0.16	1.18 $\pm$ 0.22	0.09 $\pm$ 0.34
6	0.23	-20.44 $\pm$ 0.03	36.94 $\pm$ 1.54	13.78 $\pm$ 0.44	6.66 $\pm$ 0.34	48.73 $\pm$ 6.3	2.18 $^{-0.14}_{+0.16}$	8.82 $\pm$ 0.02	2.32 $\pm$ 0.07	0.07 $\pm$ 0.07
7	0.421	-21.14 $\pm$ 0.08	47.31 $\pm$ 1.79	11.68 $\pm$ 0.77	31.55 $\pm$ 0.54	...	...	8.47 $\pm$ 0.07	3.73 $\pm$ 0.24	0.21 $\pm$ 0.12
8	0.351	-20.2 $\pm$ 0.06	21.52 $\pm$ 2.07	5.90 $\pm$ 0.87	1.32 $\pm$ 0.75	170.61 $^{-14.74}_{+13.57}$	4.16 $^{-0.48}_{+0.38}$	8.72 $\pm$ 0.12	0.79 $\pm$ 0.12	0.000 $\pm$ 0.28
9	0.5	-23.02 $\pm$ 0.04	54.97 $\pm$ 2.09	16.60 $\pm$ 1.06	15.78 $\pm$ 0.59	...	...	8.70 $\pm$ 0.05	29.68 $\pm$ 1.89	0.000 $\pm$ 0.11
10	0.598	-21.35 $\pm$ 0.13	15.19 $\pm$ 1.85	5.13 $\pm$ 1.42	14.53 $\pm$ 0.65	...	...	8.57 $\pm$ 0.24	1.99 $\pm$ 0.55	0.62 $\pm$ 0.46
11	0.348	-20.02 $\pm$ 0.13	32.87 $\pm$ 2.81	4.61 $\pm$ 1.11	4.38 $\pm$ 0.74	...	...	...	...	...
12	0.225	-19.08 $\pm$ 0.18	55.68 $\pm$ 2.42	9.94 $\pm$ 0.87	29.67 $\pm$ 0.62	...	...	...	...	...
13	0.651	-22.31 $\pm$ 0.13	52.66 $\pm$ 0.85	18.99 $\pm$ 0.49	18.47 $\pm$ 0.31	...	...	8.76 $\pm$ 0.02	17.71 $\pm$ 0.46	0.11 $\pm$ 0.04
14	0.237	-21.84 $\pm$ 0.18	16.59 $\pm$ 1.11	2.42 $\pm$ 0.9	2.20 $\pm$ 0.26	228.3 $\pm$ 12.4	11.8 $\pm$ 0.48	...	...	...
15	0.71	-21.68 $\pm$ 0.16	51.89 $\pm$ 2.52	14.96 $\pm$ 1.00	12.92 $\pm$ 0.59	176.66 $\pm$ 41.05	3.16 $\pm$ 0.13	8.69 $\pm$ 0.05	7.84 $\pm$ 0.53	0.02 $\pm$ 0.12
16	0.66	-21.18 $\pm$ 0.14	37.96 $\pm$ 1.85	9.85 $\pm$ 0.87	11.28 $\pm$ 1.07	126.28 $^{-9.6}_{+9.39}$	3.4 $^{-0.18}_{+0.16}$	8.62 $\pm$ 0.08	3.26 $\pm$ 0.29	0.03 $\pm$ 0.16
17	0.585	-22.11 $\pm$ 0.12	20.63 $\pm$ 0.87	9.77 $\pm$ 0.68	4.55 $\pm$ 0.29	244.17 $\pm$ 66.07	4.47 $\pm$ 0.46	8.89 $\pm$ 0.02	7.59 $\pm$ 0.53	0.12 $\pm$ 0.10
18	0.487	...	38.57 $\pm$ 0.53	19.61 $\pm$ 0.64	74.54 $\pm$ 2.48	...	...	8.59 $\pm$ 0.03	...	...
19	0.653	-21.2 $\pm$ 0.13	58.73 $\pm$ 1.77	21.14 $\pm$ 1.09	16.69 $\pm$ 1.39	155.08 $\pm$ 19.75	4.57 $^{-0.14}_{+0.05}$	8.78 $\pm$ 0.03	7.13 $\pm$ 0.37	0.08 $\pm$ 0.09
20	0.318	-21.08 $\pm$ 0.26	35.21 $\pm$ 2.98	9.75 $\pm$ 1.01	7.56 $\pm$ 0.81	168.17 $^{-11.18}_{+12.6}$	5.97 $^{-0.28}_{+0.33}$	8.68 $\pm$ 0.09	2.95 $\pm$ 0.30	0.17 $\pm$ 0.20
21	0.401	-20.39 $\pm$ 0.22	75.73 $\pm$ 7.02	16.94 $\pm$ 1.21	34.78 $\pm$ 1.58	114.02 $^{-13.91}_{+12.4}$	2.47 $\pm$ 0.2	8.48 $\pm$ 0.09	2.72 $\pm$ 0.19	0.000 $\pm$ 0.17
22	0.335	-20.41 $\pm$ 0.07	45.44 $\pm$ 3.30	11.97 $\pm$ 0.99	10.28 $\pm$ 0.82	87.52 $^{-12.4}_{+7.16}$	3.46 $\pm$ 0.18	8.66 $\pm$ 0.08	1.96 $\pm$ 0.16	0.000 $\pm$ 0.17
23	0.46	-20.53 $\pm$ 0.06	56.79 $\pm$ 1.66	16.32 $\pm$ 0.75	20.65 $\pm$ 0.72	...	...	8.65 $\pm$ 0.04	2.98 $\pm$ 0.14	0.01 $\pm$ 0.08
24	0.599	-21.83 $\pm$ 0.12	12.61 $\pm$ 0.94	7.21 $\pm$ 0.99	1.14 $\pm$ 0.90	...	...	8.96 $\pm$ 0.02	4.33 $\pm$ 0.59	0.14 $\pm$ 0.17
25	0.196	-19.99 $\pm$ 0.18	42.01 $\pm$ 1.98	8.19 $\pm$ 0.39	9.47 $\pm$ 0.33	125.16 $\pm$ 5.22	4.03 $\pm$ 0.2	8.49 $\pm$ 0.06	0.91 $\pm$ 0.04	0.08 $\pm$ 0.11
26	0.335	-19.56 $\pm$ 0.04	63.67 $\pm$ 3.26	16.80 $\pm$ 0.96	19.79 $\pm$ 0.66	...	...	8.63 $\pm$ 0.05	1.26 $\pm$ 0.07	0.05 $\pm$ 0.11
27	0.47	-21.62 $\pm$ 0.04	33.07 $\pm$ 0.95	12.10 $\pm$ 0.68	5.93 $\pm$ 0.43	180.38 $\pm$ 8.1	3.96 $\pm$ 0.4	8.81 $\pm$ 0.03	5.99 $\pm$ 0.34	0.000 $\pm$ 0.09
28	0.655	-21.79 $\pm$ 0.08	3.69 $\pm$ 4.15	2.65 $\pm$ 1.69	3.30 $\pm$ 3.71	...	...	8.88 $\pm$ 0.25	1.53 $\pm$ 0.98	0.83 $\pm$ 1.45
29	0.286	-20.02 $\pm$ 0.17	4.94 $\pm$ 1.72	0.77 $\pm$ 0.48	1.06 $\pm$ 0.81	...	...	...	...	...
30	0.302	-19.61 $\pm$ 0.06	23.27 $\pm$ 2.73	4.33 $\pm$ 3.18	3.12 $\pm$ 0.95	...	...	8.49 $\pm$ 0.79	0.34 $\pm$ 0.25	0.000 $\pm$ 1.26
31	0.658	-21.67 $\pm$ 0.13	30.45 $\pm$ 0.89	17.50 $\pm$ 1.08	9.32 $\pm$ 1.16	...	...	8.92 $\pm$ 0.01	9.08 $\pm$ 0.56	0.11 $\pm$ 0.08
32	0.447	-21.26 $\pm$ 0.07	52.39 $\pm$ 0.95	15.27 $\pm$ 0.62	25.79 $\pm$ 0.76	...	...	8.62 $\pm$ 0.03	5.44 $\pm$ 0.22	0.03 $\pm$ 0.07
33	0.388	-20.16 $\pm$ 0.08	13.39 $\pm$ 1.09	8.41 $\pm$ 0.77	2.24 $\pm$ 0.86	...	...	8.97 $\pm$ 0.01	1.09 $\pm$ 0.10	0.14 $\pm$ 0.13
34	0.387	-20.22 $\pm$ 0.07	52.68 $\pm$ 1.95	14.32 $\pm$ 1.15	32.74 $\pm$ 1.38	148.69 $^{-9.73}_{+22.4}$	4.48 $\pm$ 0.3	8.54 $\pm$ 0.08	1.97 $\pm$ 0.16	0.05 $\pm$ 0.14
35	0.447	-20.14 $\pm$ 0.08	39.93 $\pm$ 2.32	13.68 $\pm$ 1.32	11.12 $\pm$ 3.14	210.19 $^{-22.4}_{+19.7}$	2.69 $\pm$ 0.14	8.76 $\pm$ 0.07	1.75 $\pm$ 0.17	0.000 $\pm$ 0.18
36	0.35	-20.11 $\pm$ 0.09	46.43 $\pm$ 1.22	12.96 $\pm$ 0.8	17.01 $\pm$ 0.5	...	...	8.64 $\pm$ 0.05	1.61 $\pm$ 0.10	0.000 $\pm$ 0.10
37	0.397	-20.97 $\pm$ 0.07	19.89 $\pm$ 0.71	10.17 $\pm$ 0.66	3.37 $\pm$ 0.29	...	...	8.92 $\pm$ 0.01	2.78 $\pm$ 0.18	0.12 $\pm$ 0.08
38	0.476	-21.51 $\pm$ 0.07	28.38 $\pm$ 1.19	10.05 $\pm$ 0.56	7.26 $\pm$ 0.62	...	...	8.78 $\pm$ 0.03	4.50 $\pm$ 0.25	0.09 $\pm$ 0.09
39	0.345	-19.73 $\pm$ 0.06	21.7 $\pm$ 4.	4.36 $\pm$ 3.24	1.87 $\pm$ 0.70	...	...	8.55 $\pm$ 0.74	0.38 $\pm$ 0.28	0.15 $\pm$ 1.29
40	0.37	-20.15 $\pm$ 0.09	39.27 $\pm$ 2.77	9.42 $\pm$ 1.24	14.77 $\pm$ 1.28	144.26 $^{-17.14}_{+14.92}$	4.07 $^{-0.3}_{+0.26}$	8.55 $\pm$ 0.13	1.21 $\pm$ 0.16	0.24 $\pm$ 0.24
41	0.371	-20.56 $\pm$ 0.05	22.08 $\pm$ 1.89	5.14 $\pm$ 1.09	9.08 $\pm$ 1.06	188.34 $^{-19.37}_{+19.54}$	8.71 $^{-0.82}_{+1.15}$	8.52 $\pm$ 0.21	0.96 $\pm$ 0.20	0.19 $\pm$ 0.37
42	0.464	-20.32 $\pm$ 0.14	13.07 $\pm$ 1.86	6.38 $\pm$ 1.01	3.43 $\pm$ 1.05	...	...	8.89 $\pm$ 0.05	0.96 $\pm$ 0.15	0.13 $\pm$ 0.25
43	0.444	-21.12 $\pm$ 0.2	27.44 $\pm$ 1.24	10.12 $\pm$ 0.84	7.73 $\pm$ 0.64	...	...	8.79 $\pm$ 0.04	3.17 $\pm$ 0.26	0.14 $\pm$ 0.13
44	0.397	-20.03 $\pm$ 0.08	14.31 $\pm$ 2.10	5.46 $\pm$ 1.20	2.17 $\pm$ 0.84	195.81 $^{-10.35}_{+13.33}$	4.23 $^{-0.23}_{+0.31}$	8.84 $\pm$ 0.10	0.63 $\pm$ 0.14	0.03 $\pm$ 0.35

lier stages of the assembly of their content of metals, as indicated by their low oxygen abundances. This suggests that they are probably also at earlier stages of assembling their stellar masses, as both stellar and metal contents of galaxies are thought to be linked. Metal-poor luminous galaxies at intermediate redshift are therefore expected to deviate from the local baryonic Tully-Fisher relation.

Hammer et al. (2005) have presented a body of evidence to show that present-day intermediate stellar mass galaxies, i.e., with stellar masses of  $3-30 \times 10^{10} M_\odot$ , have built up half of their stellar mass since  $z \sim 1$ , and emphasize the importance of luminous infrared galaxies, thought to be starbursts resulting from merging at these masses. The star

formation in luminous infrared galaxies accounts for most of the stellar mass growth in these galaxies since  $z \sim 1$ . They argue that recent merging and gas infall explain both star formation history and morphological changes in a hierarchical galaxy formation scheme, where more than 50 per cent of spiral galaxies experienced their last major merger event less than 8 Gyr ago. Intermediate redshift luminous infrared galaxies show oxygen abundances two times lower than local bright disk galaxies (Liang et al. 2004). The presence of a population of intermediate redshift massive and luminous galaxies with oxygen abundances lower than those observed locally for similar galaxies, supports the scenario



**Table 1.** Coordinates of the objects in our sample of field galaxies

ID	R.A. (J2000)	Dec. (J2000)
1	02:39:57.8	-01:33:10
2	02:39:51.8	-01:35:21
3	02:39:48.1	-01:38:16
4	02:40:03.6	-01:37:56
5	02:39:54.5	-01:35:04
6	02:40:00.9	-01:36:16
7	02:40:06.7	-01:36:55
8	22:58:33.7	-34:47:43
9	22:58:41.9	-34:47:21
10	00:56:59.1	-27:40:41
11	00:56:48.2	-27:40:13
12	00:56:48.6	-27:40:01
13	00:56:58.9	-27:43:53
14	00:56:46.3	-27:42:50
15	00:56:50.9	-27:38:01
16	00:56:47.2	-27:38:33
17	00:56:55.6	-27:39:08
18	00:57:11.5	-27:39:48
19	00:57:07.9	-27:39:28
20	04:43:06.7	+02:12:15
21	04:43:14.4	+02:10:30
22	20:56:23.2	-04:34:41
23	20:56:22.4	-04:37:49
24	20:56:20.2	-04:37:50
25	20:56:22.6	-04:41:32
26	20:56:24.4	-04:39:53
27	10:57:01.2	-03:34:20
28	00:18:32.8	+16:22:18
29	00:18:27.0	+16:26:59
30	00:18:32.1	+16:25:22
31	00:18:32.8	+16:26:10
32	00:18:15.6	+16:25:05
33	00:18:17.2	+16:25:34
34	00:18:21.0	+16:26:14
35	00:18:19.2	+16:25:44
36	00:18:18.2	+16:23:58
37	00:18:37.8	+16:24:56
38	16:23:42.6	+26:31:14
39	16:23:36.0	+26:34:17
40	16:23:40.1	+26:34:05
41	20:56:19.6	-04:38:48
42	20:56:24.9	-04:37:38
43	20:56:25.2	-04:36:00
44	20:56:32.5	-04:36:27

in which the assembly of intermediate stellar mass galaxies is still operating between  $z \sim 1$  and  $z = 0$ .

The sample studied in this paper is by no means complete. It is not possible therefore to assess the implication of our findings for constraining galaxy assembly from  $z \sim 1$  to the present epoch. Additional work to determine the properties of metal-poor massive galaxies and their evolution, e.g., number density, stellar masses, morphologies, and stellar mass function, is needed to help reveal the nature of star formation during the last  $\sim 8$  Gyr. In the near future it will be possible to conduct further studies to measure chemical properties and stellar masses of star-forming galaxies at intermediate redshifts, in order to tightly constrain the assembly of the stellar and metal content of present day galaxies. Large galaxy surveys like DEEP2 (Davis et al. 2003) and EDisCS (White et al. 2005) are promising, as they will ob-

serve large samples of galaxies distributed over a wide area and redshift range.

## 6 SUMMARY & CONCLUSIONS

We have used spectrophotometric data for a sample of luminous ( $M_B \lesssim -19$ ), mostly disk, field galaxies in the redshift range  $0.2 \lesssim z \lesssim 0.8$ , with measured maximum rotation velocities and emission scale lengths, to investigate the properties of the interstellar emitting gas of massive galaxies at intermediate redshift.

Emission line equivalent widths and excitation- and metallicity-sensitive emission line diagnostic ratios of the massive star-forming galaxies in our sample cover similar ranges to those observed for local emission line galaxies over a wide range of luminosities, i.e.,  $-14.0 \lesssim M_B \lesssim -22.0$ . The properties of the interstellar emitting gas for a subsample of massive and luminous field galaxies at intermediate redshifts are similar to those observed for faint and metal-poor galaxies, with moderate excitation-sensitive diagnostic ratios, at the present cosmic epoch.

The oxygen abundance of interstellar emitting gas has been estimated using the “strong-line” method. These estimated oxygen abundances range from 8.4 to 9.0 in units of  $12 + \log(\text{O}/\text{H})$ . Our sample galaxies exhibit a luminosity–metallicity relation different from that of local galaxies. A subsample of massive galaxies show oxygen abundances that are consistent with what is observed locally for their local counterparts. However, a fraction of massive star-forming galaxies in our sample have low oxygen abundances that are observed locally only for much fainter galaxies, in agreement with the findings of other recent investigations of the chemical properties of star-forming galaxies at intermediate redshifts (Kobulnicky et al. 2003; Liang et al. 2004; Maier et al. 2005). Oxygen abundances are not found to correlated with either the maximum rotation velocity nor with the emission scale length size of the galaxy.

Luminous and large field galaxies at intermediate redshifts show similar extinction-uncorrected and intrinsic star formation rates to their local counterparts, independent of their gas phase oxygen abundances. The nebular extinction as derived from the ratio of the extinction-uncorrected star formation rates based on  $[\text{OII}]\lambda 3727$  and  $\text{H}\beta$ , respectively, is found to span a similar range to that for star-forming galaxies at the present epoch, but has a lower mean than is observed locally for optically-selected galaxy samples. Intermediate redshift luminous metal-rich galaxies exhibit similar internal reddening and intrinsic star formation rate to local bright metal-rich galaxies, while luminous metal-poor galaxies show lower internal reddening, similar to what is observed locally for faint metal-poor galaxies, but similar intrinsic star formation rate to metal-rich galaxies.

The relationship between gas phase oxygen abundance and colour excess for intermediate redshift galaxies is similar to that observed at the present epoch. The best interpretation for this is that the dust obscuration is regulated more by galaxy metal content than luminosity.

The diversity of the properties of massive and large galaxies at intermediate redshifts supports the scenario whereby galaxies are still assembling their baryonic content between  $z \sim 1$  and  $z = 0$ . Intermediate redshift massive

and large galaxies with low gas phase oxygen abundances are most likely immature galaxies that will increase their metallicities and their stellar masses to the present epoch.

## ACKNOWLEDGMENTS

This work was based on observations made with ESO Telescopes at Paranal Observatory under programme IDs 066.A-0376 and 069.A-0312, and on observations made with the NASA/ESA *Hubble Space Telescope*, obtained from the data archive at the Space Telescope Institute. STScI is operated by the association of Universities for Research in Astronomy, Inc. under the NASA contract NAS 5-26555.

## REFERENCES

- Afonso J., Hopkins A., Mobasher B., Almeida C., 2003, *ApJ*, 597, 269
- Allende Prieto C., Lambert D.L., Asplund, M. 2001, *ApJ*, 556, L63
- Alloin D., Collin-Souffrin S., Joly M., Vigroux L., 1979, *A&A*, 78, 200
- Aragón-Salamanca A., Ellis R. S., Couch W. J., Carter D., 1993, *MNRAS*, 262, 764
- Baldwin J.A., Phillips M.M., Terlevich R., 1981, *PASP*, 93, 5
- Bamford S. P., Milvang-Jensen B., Aragón-Salamanca A., Simard L., 2005, *MNRAS*, 361, 109
- Bamford S. P., Aragón-Salamanca A., Milvang-Jensen B., 2006, *MNRAS*, 366, 308
- Brinchmann J., Ellis R.S., 2000, *ApJ*, 536L, 77
- Buat V., Boselli A., Gavazzi G., Bonfanti C., 2002, *A&A*, 383, 801
- Bundy K., Ellis R.S., Conselice C.J., 2005, *ApJ*, 625, 621
- Cardelli J.A., Clayton G.C., Mathis J.S., 1989, *ApJ*, 329, 33
- Conselice C.J., Bundy K., Ellis R.S., Brinchmann J., Vogt N.P., Phillips A.C., 2005, *ApJ*, 628, 160
- Cowie L.L., Hu E.M., Songaila A., Egami E., 1997, *ApJ*, 481, L9
- Davis, M., et al., 2003, *Proc. SPIE*, 4834, 161
- Denicoló G., Terlevich R., Terlevich E., 2002, *MNRAS*, 330, 69
- Dessauges-Zavadsky M., Pindao M., Maeder A., Kunth D., 2000, *A&A*, 355, 89
- Drory N., Bender R., Feulner G., Hopp U., Maraston C., Snigula J., Hill G.J., 2004, *ApJ*, 608, 742
- Ellison, S.L., Kewley L.J., Mallén-Ornelas G., 2005, *MNRAS*, 357, 354
- Erb D.K., Shapely A.E., Steidel C.C., et al., 2003, *ApJ*, 591, 101
- Flores H., et al., 2005, in *The fabulous destinay of galaxies: bridging past and present*, in press.
- Fontana A., et al., 2004, *A&A*, 424, 23
- Fukugita M., Shimasaku K., Ichikawa T., 1995, *PASP*, 107, 945
- Gallagher J.S., Bushouse H., Hunter D.A., 1989, *ApJ*, 97, 700
- Guzmán R., Gallego J., Koo D.C., et al. 1997, *ApJ*, 489, 559
- Hammer F., Gruel N., Thuan T.X., Flores H., Infante L., 2001, *ApJ*, 550, 570
- Hammer F., Flores H., Elbaz D., Zheng X.Z., Liang Y.C., Cesarsky C., 2005, *A&A*, 430, 115
- Hippelein H., Maier C., Meisenheimer K., et al., 2003, *A&A*, 402, 65
- Hogg D.W., Cohen J.G., Blandford R., Pahre M.A., 1998, *ApJ*, 504, 622
- Hopkins A., Connolly A., Haarsma D., Cram L., 2001, *AJ*, 122, 288
- Hopkins A.M., Miller C.J., Nichol R.C., et al., 2003, *ApJ*, 599, 971
- Huchra J.P., Davis M., Latham D., & Tonry J. 1983, *ApJS*, 52, 89
- Im M., Simard L., Faber S.M., et al., 2002, *ApJ*, 571, 136
- Jansen, R.A., Fabricant, D., Franx, M., & Caldwell, N., 2000, *ApJS*, 126, 331
- Jansen R.A., Franx M., Fabricant D., 2001, *ApJ*, 551, 825
- Kashikawa N., et al., 2002, *PASJ*, 54, 819
- Kennicutt R.C., Jr. 1992, *ApJ*, 388, 310
- Kennicutt R.C., Jr. 1998, *ARA&A*, 36, 189
- Kennicutt R.C., Jr., Bresolin F., Garnett D.R., 2003, *ApJ*, 591, 801
- Kewley L. J., Heisler C. A., Dopita M. A., Lumsden S., 2001, *ApJS*, 132, 37
- Kewley L.J., Dopita M.A., 2002, *ApJS*, 142, 35
- Kewley, L.J., Geller, M., & Jansen, R.A., 2004, *AJ*, 127, 2002
- Kobulnicky H. A., Kennicutt Jr. R. C., Pizagno J. L., 1999, *ApJ*, 514, 544
- Kobulnicky H.A., Zaritsky D., 1999, *ApJ*, 511, 118
- Kobulnicky H.A., Koo D.C., 2000, *ApJ*, 545, 712
- Kobulnicky H. A., et al. 2003, 599, 1006
- Kobulnicky H. A., Phillips A. C., 2003, *ApJ*, 599, 1031
- Kobulnicky H. A., & Kewley L.J., 2004, *ApJ*, 617, 240
- Kong X., Cheng F.Z., Weiss A., Charlot S., 2002, *A&A*, 396, 503
- Kong X., 2004, *A&A*, 425, 417
- Lamareille F., Mouhcine M., Contini T., Lewis I.J., Maddox S.J., 2004, *MNRAS*, 350, 396
- Lequeux J., Peimbert M., Rayo J.F., et al., 1979, *A&A*, 80, 155
- Lemoine-Busserolle M., Contini T., Pello R., Le Borgne J.-F., Kneib J.-P., Lidman C., 2003, *A&A*, 397, 839
- Liang Y.C., Hammer F., Flores H., Gruel N., Assémat F., 2004, *A&A*, 417, 905
- Lilly S.J., Carollo C.M., Stockton A.N., 2003, *ApJ*, 597, 730
- Maier C., Meisenheimer K., Hippelein H., 2004, *A&A*, 418, 475
- Maier C., Lilly S.J., Carollo M., Stockton A., Brodwin M., 2005, *ApJ*, 634, 849
- Maier C., Lilly S.J., Carollo M., Meisenheimer K., Hippelein H., Stockton A., 2006, *ApJ*, 639, 858
- McCall M.L., Rybski P.M., Shields G.A., 1985, *ApJS*, 57, 1
- McGaugh S. S., 1991, *ApJ*, 380, 140
- McGaugh S. S., 1994, *ApJ*, 426, 135
- Mehlert D., Noll S., Appenzeller I., et al., 2002, *A&A*, 393, 809
- Melbourne J., Salzer J. J., 2002, *AJ*, 123, 2302
- Milvang-Jensen B., Aragón-Salamanca A. Hau G. K. T.,

- Jørgensen I. Hjorth J., 2003, 339L, 1  
Milvang-Jensen B., 2003, Ph.D thesis, Univ. of Nottingham  
Mouhcine M., Contini T., 2002, A&A, 389, 106  
Mouhcine M., Lewis I.J., Jones J.B., Lamareille F., Maddox S.J., Contini T., 2005, MNRAS, in press  
Nakamura O., Fukugita M., Brinkmann J., Schneider D.P., 2004, AJ, 127, 2511  
Nakamura, O., Aragón-Salamanca, A., Milvang-Jensen, B., Arimoto, N., Ikuta, C., Bamford, S. P., 2006, MNRAS, 366, 144  
Osterbrock D.E., 1989, *Astrophysics of Gaseous Nebulae and Active Galactic Nuclei* (Mill Valley: Univ. Sci.)  
Pagel B.E.J., Edmunds M.G., Blackwell D.E., Chum M.S., Smith G., 1979, MNRAS, 189, 95  
Pettini M., Kellogg M., Steidel C.C., Dickinson M., Adelberger K.L., Giavalisco M., 1998, ApJ, 508, 539  
Pettini M., Shapley A. E., Steidel C. C., et al., 2001, ApJ, 554, 981  
Pilyugin L. S., 2001, A&A, 374, 412  
Rola C. S., Terlevich E., Terlevich R. J., 1997, MNRAS, 289, 419  
Rosa-González D., Terlevich E., Terlevich R., 2002, MNRAS, 332, 283  
Salzer J.J., MacAlpine G.M., Boroson T.A., 1989, ApJS, 70, 479  
Seifert W., et al., 2000, in Iye M., Moorwood, A. F., eds, Proc. SPIE Vol. 4008, *Optical and IR Telescope Instrumentation and Detectors* p. 96  
Simard L., Pritchett C.J., 1998, ApJ, 505, 96  
Simard L., Pritchett C.J., 1999, ApJ, 111, 453  
Skillman E.D., Kennicutt R.C., Hodge P.W., 1989, ApJ, 347, 875  
Spergel D.N., et al., 2003, ApJS, 148, 175  
Stasińska G., 1990, A&AS, 83, 501  
Stasińska G., Sodr e L., Jr., 2001, A&A, 374, 919  
Stasińska G., Mateus A., Jr., Sodr e L., Jr., Szczerba R., 2004, A&A, 420, 475  
Sullivan M. Mobasher B., Chan B., Cram L., Ellis R., Treyer M., Hopkins A., 2001, ApJ, 558, 72  
Thompson D.J., Djorgovski S., 1991, ApJ, 371, 55  
Tremonti C.A., Heckman T.M., Kauffmann G., et al., 2004, ApJ, 613, 898  
van Dokkum P.G., Ellis R.S., 2003, ApJ, 592, 53  
van Zee L., Salzer J.J., Haynes M.P., O'Donoghue A.A., Balonek T.J., 1998, AJ, 116, 2805  
Veilleux S., Osterbrock D. E., 1987, ApJS, 63, 295  
Wang B., Heckman T.M., 1996, ApJ, 457, 645  
White S.D.M., et al. 2005, A&A, in press (astro-ph/0508351)  
Zaritsky D., Kennicutt R.C., Huchra J.P, 1994, ApJ, 420, 87  
Ziegler B.L., Bohm A., Fricke, et al., 2002, ApJ, 564, 69